Perlecan domain V is neuroprotective and proangiogenic following ischemic stroke in rodents

Boyeon Lee,[1] Douglas Clarke,[1] Abraham Al Ahmad,[1,2] Michael Kahle,[1] Christi Parham,[1] Lisa Auckland,[1] Courtney Shaw,[1] Mehmet Fidanboylu,[3] Anthony Wayne Orr,[4] Omolara Ogunshola,[2] Andrzej Fertala,[5] Sarah A. Thomas,[3] and Gregory J. Bix[1,6]

[1]Department of Molecular and Cellular Medicine, Texas A&M College of Medicine, College Station, Texas, USA. [2]Institute of Veterinary Physiology, Vetsuisse Faculty, University of Zurich, Zurich, Switzerland. [3]King's College London, Institute of Pharmaceutical Science, London, United Kingdom. [4]Department of Pathology, Louisiana State University Health Science Center, Shreveport, Louisiana, USA. [5]Department of Dermatology and Cutaneous Biology, Thomas Jefferson University, Philadelphia, Pennsylvania, USA. [6]Neuroscience and Experimental Therapeutics, Texas A&M College of Medicine, College Station, Texas, USA.

Stroke is the leading cause of long-term disability and the third leading cause of death in the United States. While most research thus far has focused on acute stroke treatment and neuroprotection, the exploitation of endogenous brain self-repair mechanisms may also yield therapeutic strategies. Here, we describe a distinct type of stroke treatment, the naturally occurring extracellular matrix fragment of perlecan, domain V, which we found had neuroprotective properties and enhanced post-stroke angiogenesis, a key component of brain repair, in rodent models of stroke. In both rat and mouse models, Western blot analysis revealed elevated levels of perlecan domain V. When systemically administered 24 hours after stroke, domain V was well tolerated, reached infarct and peri-infarct brain vasculature, and restored stroke-affected motor function to baseline pre-stroke levels in these multiple stroke models in both mice and rats. Post-stroke domain V administration increased VEGF levels via a mechanism involving brain endothelial cell $\alpha5\beta1$ integrin, and the subsequent neuroprotective and angiogenic actions of domain V were in turn mediated via VEGFR. These results suggest that perlecan domain V represents a promising approach for stroke treatment.

Introduction

Ischemic stroke, a condition resulting from occlusion of brain vasculature (1), manifests as an ischemic core of rapid cell death, surrounded by a vulnerable penumbral region (2). Within the penumbra, reparative revascularization (angiogenesis) and neuronal repopulation (neurogenesis) occur in close proximity, facilitating mutually supportive neuron–endothelial cell crosstalk (3). Additionally, angiogenic blood vessels serve as a physical scaffold for neurons to migrate toward the ischemic core (4). Collectively, this neurovascular coupling represents a means of post-stroke repair ripe for therapeutic exploitation. Indeed, recent experimental therapies such as pharmaceuticals, stem cells, and growth factors have attempted to capitalize on neurovascular repair concepts to promote stroke recovery (5, 6). However, pharmaceutical and growth factor therapies raise questions of potentially serious systemic side effects, drug interactions, and contra-indications. Similarly, cell-based therapies raise important safety issues, including the potential for cancerous transformation.

Additionally, many factors that prevent cell death also inhibit repair, or vice versa, depending upon when they are administered after stroke. For example, NMDA receptor antagonists and protease inhibitors are both neuroprotective and detrimental to repair. VEGF further disrupts blood-brain barrier stability, promotes brain edema, and enhances hemorrhagic transformation and brain infarct size if administered acutely (7), but is neuroprotective and enhances angiogenesis and neurogenesis when given chronically (8, 9). Thus, there is a clear need for a stroke therapy that is both neuroprotective and promotes brain repair. This need is underscored by the fact that the one FDA-approved stroke therapy, TPA, has a narrow therapeutic window of 3–4.5 hours after ischemic stroke onset.

We hypothesized that neuroprotection and brain repair might both be enhanced by treatment with a factor generated endogenously by injury and the reparative process itself. We further reasoned that the vascular extracellular matrix, a biologic interface between vascular and other brain tissue that is actively proteolyzed during both the initial injury and subsequent repair response (10), was a logical place to look for factors with therapeutic potential. In particular, the vascular extracellular matrix proteoglycan component perlecan undergoes greater acute (within 1–2 hours of stroke onset) and chronic (up to 7 days) proteolysis after stroke (in the non-human primate) than any other extracellular matrix component studied (11). Furthermore, perlecan is required for brain angiogenesis (12). Interestingly, perlecan also contains the antiangiogenic C-terminal protein fragment domain V (DV, also known as endorepellin; ref. 13), which is activated by proteolysis from full-length perlecan (10). However, DV has not been studied in the brain due to the absence of its previously identified antiangiogenic receptor from angiogenic brain endothelial cells (13–15). In this study, using two different stroke models in mice and rats, we have demonstrated a stable and long-lasting increase in brain DV concentrations following stroke injury. We further demonstrate that this endogenous DV could play a role in the brain's response to stroke, inasmuch as DV-deficient mice experience larger infarcts

Authorship note: Boyeon Lee and Douglas Clarke contributed equally to this work.
Conflict of interest: The authors have declared that no conflict of interest exists.
Citation for this article: *J Clin Invest.* 2011;121(8):3005–3023. doi:10.1172/JCI46358.

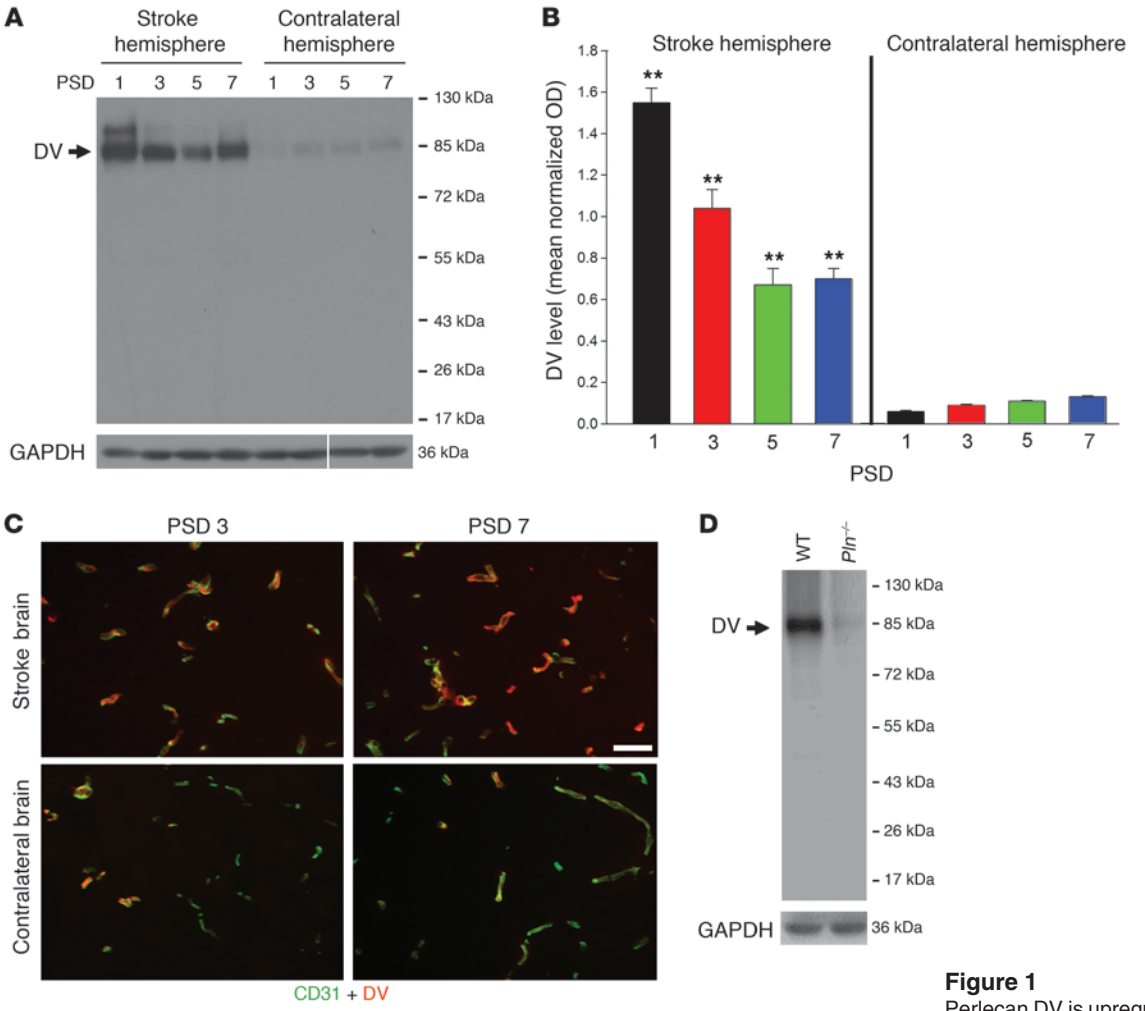

Figure 1

Perlecan DV is upregulated after stroke in rodents. (**A**) Anti-DV Western blot analysis of post-stroke rat brain, with GAPDH internal loading control. DV levels were assessed in both ipsilateral (stroke) and contralateral hemispheres on the post-stroke days as labeled. GAPDH loading control lanes on contralateral PSD 5 and 7 were run on the same gel but were noncontiguous. (**B**) Densitometry analysis of DV Western blot as shown in **A**. DV band density intensities were normalized to their respective GAPDH bands (**P < 0.01 between ipsi- and contralateral hemispheres for each PSD, n = 15 per PSD). (**C**) DV and CD31 co-immunohistochemistry of rat stroke and corresponding contralateral brain tissue on PSD 3 and 7. Scale bar: 50 μM. (**D**) Anti-DV Western blot analysis of PSD 3 brain tissue from WT littermate mice and *Pln*$^{-/-}$ mice, with GAPDH as internal loading control. (**E**) Plot of mean ischemic lesion volumes of stroke WT mice and *Pln*$^{-/-}$ mice (**P < 0.01 between groups on each PSD, n = 15 per group per PSD). (**F**) WT or *Pln*$^{-/-}$ mouse brain TTC staining at PSD 3. Yellow asterisks indicate ischemic lesions (TTC-negative, appears white).

Table 1
DV treatment does not alter vital signs, blood gases, or serum electrolytes

Measured physiologic parameters	PBS-treated (mean ± SD)	DV-treated (mean ± SD)
Systolic blood pressure (mmHg)	114.1 ± 2.4	113.9 ± 3.0
Heart rate (bpm)	300 ± 27.75	299.71 ± 27.17
Breathe rate (BrPM)	105.58 ± 12.85	108.62 ± 13.83
Partial pressure O_2 (mmHg)	165.1 ± 35.5	171.1 ± 16.1
Partial pressure CO_2 (mmHg)	54.9 ± 10.9	51.1 ± 1.4
Hematocrit (%)	34.7 ± 3.9	33.2 ± 6.5
Sodium (mEq/l)	150.3 ± 3.3	152.8 ± 1.5
Potassium (mEq/l)	6.4 ± 0.9	6.4 ± 0.8
Ionized calcium (mg/dl)	5.2 ± 0.3	5.2 ± 0.04
Oxygen saturation %	98.6 ± 0.8	98.8 ± 0.4
pH	7.3 ± 0.02	7.3 ± 0.1

Measurements of mice (n = 10 per treatment group) taken on PSD 1, two hours after i.p. injection of PBS (baseline) or DV (total of 26 hours after stroke). No significant differences in any of these parameters was noted between PBS and DV treatment. BrPM, breaths per minute.

than their WT counterparts. Additionally, we have demonstrated that DV administered systemically 24 hours after stroke (a) is well tolerated; (b) reaches stroke core and peri-infarct vasculature; (c) is neuroprotective; (d) significantly improves post-stroke functional motor recovery to pre-stroke function via a previously unidentified DV receptor; (e) "rescues" the worsened stroke severity of DV-deficient mice; and (f) unexpectedly enhances brain angiogenesis. This latter result underscores substantial differences between brain and non-brain angiogenesis. Collectively, our results suggest that DV is a distinct, nontoxic, multi-functional stroke treatment.

Results

Perlecan DV is upregulated after stroke. Perlecan is rapidly processed after stroke in the nonhuman primate (11). Therefore, it was hypothesized that post-stroke perlecan proteolysis could increase free DV levels. In the rat, stereotactic injection of endothelin-1 was used to induce focal cerebral ischemia by transiently occluding the middle cerebral artery (MCA) (16). Compared with sham surgery controls, which demonstrated no Western blot–detectable DV in the ipsi- or contralateral hemispheres on post-stroke days (PSD) 1, 3, 5, and 7 (data not shown), stroke hemisphere DV levels were elevated at PSD 1, 3, 5, and 7 (Figure 1, A and B). Likewise, use of the transient tandem ipsilateral common carotid artery (CCA) and distal MCA occlusion stroke model in mice (ref. 17 and Supplemental Figure 1; supplemental material available online with this article; doi:10.1172/JCI46358DS1) resulted in identical (to that seen with the endothelin-1 stroke model) increased and sustained DV stroke brain concentrations as compared with sham controls (which demonstrated no Western blot–detectable DV; data not shown). Finally, a single, higher-kDa-weight (relative to DV) nonspecific band was detected in some lanes (13).

As perlecan is predominantly found in the vascular basement membrane (18), we hypothesized and demonstrated by DV and CD31 co-immunohistochemistry that DV was generated around blood vessels after stroke and was more visibly apparent than in the corresponding contralateral brain hemisphere (Figure 1C). Perlecan domain IV (DIV, immediately adjacent to DV in non-proteolyzed perlecan) (18) and DV co-immunohistochemistry on stroke brain tissue was performed to further distinguish free DV (not colocalized with DIV) from DV that did colocalize with DIV (perlecan-attached DV, Supplemental Figure 2). Collectively, these results demonstrate that post-stroke perlecan processing results in a rapid perivascular increase in stroke brain DV levels that persists to at least PSD 7.

Perlecan-deficient mice have larger ischemic stroke lesions. Having demonstrated that DV was persistently generated in the post-stroke brain, we examined its potential significance for stroke by inducing stroke in mice that express 10% of total normal perlecan (DV's parent molecule) and DV levels (hypomorphs, designated $Pln^{-/-}$) (19). Perlecan-null mice were not used, as they are embryonic lethal (20), whereas perlecan hypomorph mice are viable, fertile, and have no reported defects in the CNS (19, 21). It is important to reiterate that since these mice are 90% deficient in all of perlecan (which includes but is not limited to DV), any difference in ischemic lesion size compared with WT littermates could be attributed to a deficiency in part or all of the perlecan molecule. However, we hypothesized that a failure of perlecan deficiency to affect ischemic lesion size could suggest that DV might not play a significant role in stroke, making the $Pln^{-/-}$ mouse a good screening tool for DV's potential relevance to stroke. Furthermore, prior to using them in our stroke model, we ruled out potential differences in gross neurovascular anatomy (i.e., the ACA and MCA anastomosis number and distribution from midline as visualized via black latex intravascular injection) between $Pln^{-/-}$ mice and WT littermate controls (all in a C57BL/6 background) as a potential cause of differences in stroke severity (22, 23). No significant differences were noted in either the mean number of anastomoses (9.80 ± 1.46 per hemisphere for littermate WT and 9.74 ± 1.73 per hemisphere for $Pln^{-/-}$) or in the distance between the line of anastomoses and the midline at 2, 4, and 6 mm from the frontal pole (Supplemental Figure 3). Furthermore, as expected, DV Western blot analysis of the PSD 1 ipsilateral (stroke) brain hemisphere of the $Pln^{-/-}$ mice demonstrated a substantial deficiency in their post-stroke generation of DV (Figure 1D). Importantly, $Pln^{-/-}$ hypomorph mice had larger mean ischemic lesion volumes than WT controls on PSD 1, 2, and 3 (Figure 1, E and F), suggesting that perlecan and potentially its C-terminal DV portion could play a role in ischemic stroke injury.

Administered DV reaches stroke core and peri-infarct vasculature. We next reasoned that if endogenous DV plays a potentially beneficial role in the brain's response to stroke, as supported by the negative consequence of perlecan/DV deficiency, this role might be enhanced by administration of additional DV. To that end, we administered purified human recombinant DV, free of contamination with fibronectin (an abundant serum component that reduces brain injury following transient cerebral ischemia; Supplemental Figure 4 and ref. 24), heat-inactivated DV control, or PBS vehicle control via i.p. injection to rats and mice after transient occlusion of their left MCA. DV treatment was well tolerated in all cases as previously reported (14). Furthermore, no significant changes were noted in vital signs, blood gases, pH, and electrolytes with DV, heat-inactivated DV, or PBS treatment in rats or mice (Table 1; mouse parameters 2 hours after the first PBS or DV treatment are shown).

We first asked whether systemically administered DV could reach the site of brain stroke injury. Upon immunohistochemistry for its C-terminal HIS epitope tag (Figure 2, A and B), administered DV was found in stroke and peri-infarct brain regions (identified morphologically) in the rat but was essentially absent in

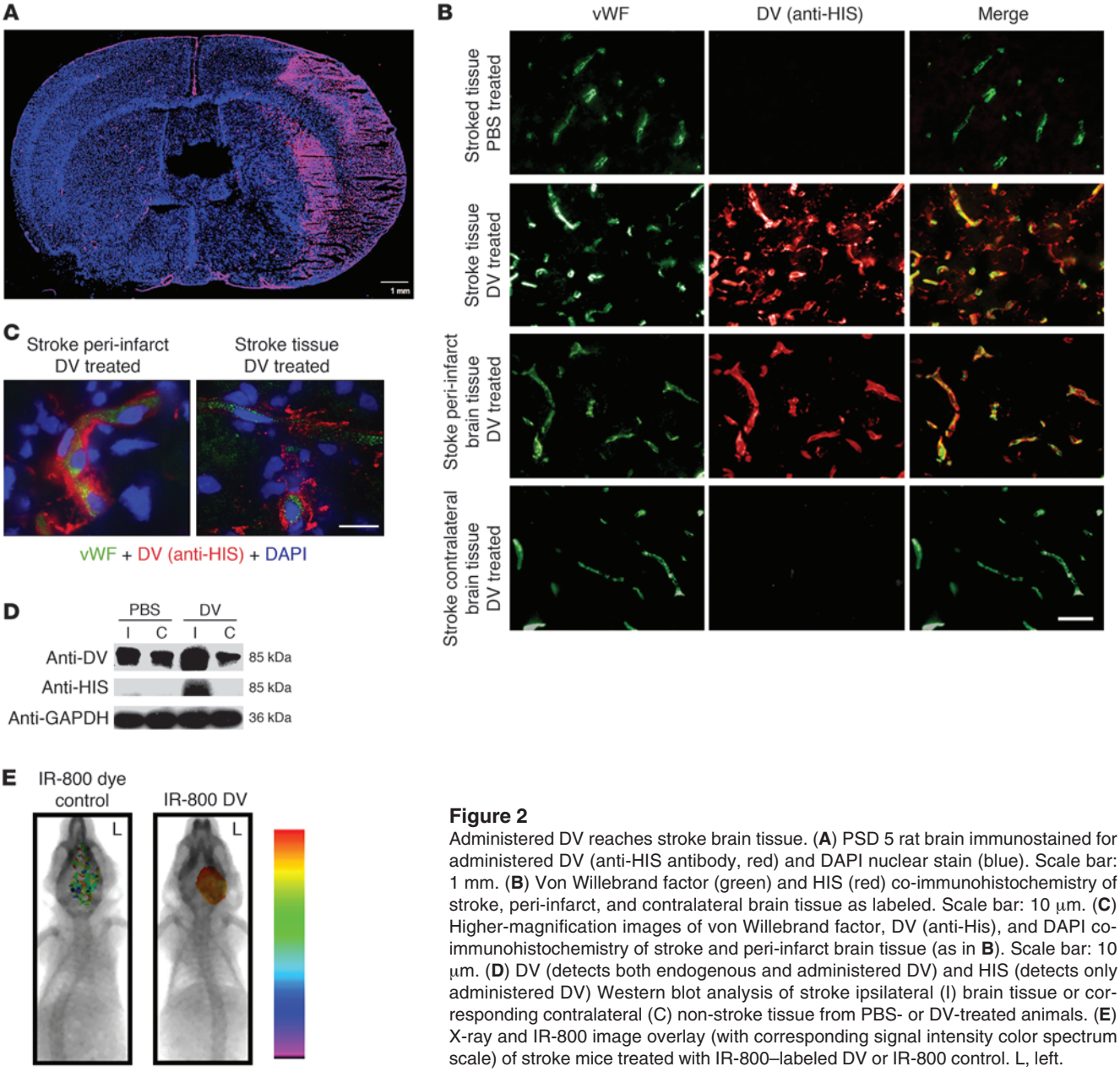

Figure 2
Administered DV reaches stroke brain tissue. (**A**) PSD 5 rat brain immunostained for administered DV (anti-HIS antibody, red) and DAPI nuclear stain (blue). Scale bar: 1 mm. (**B**) Von Willebrand factor (green) and HIS (red) co-immunohistochemistry of stroke, peri-infarct, and contralateral brain tissue as labeled. Scale bar: 10 μm. (**C**) Higher-magnification images of von Willebrand factor, DV (anti-His), and DAPI co-immunohistochemistry of stroke and peri-infarct brain tissue (as in **B**). Scale bar: 10 μm. (**D**) DV (detects both endogenous and administered DV) and HIS (detects only administered DV) Western blot analysis of stroke ipsilateral (I) brain tissue or corresponding contralateral (C) non-stroke tissue from PBS- or DV-treated animals. (**E**) X-ray and IR-800 image overlay (with corresponding signal intensity color spectrum scale) of stroke mice treated with IR-800–labeled DV or IR-800 control. L, left.

the contralateral hemisphere. Likewise, no appreciable anti-HIS immunohistochemical signal was detected in stroke animals that were not treated with DV (Figure 2B). Additionally, most of the administered DV was found in a perivascular distribution (particularly so in the peri-infarct region; Figure 2, B and C), consistent with its ability to reach solid tumor perivasculature in vivo (14). The results were similar in stroke mouse brain (data not shown). DV's ability to reach the site of stroke was further confirmed by Western blot analysis (Figure 2D). To further demonstrate that administered DV reached stroke tissue, we treated stroke mice with DV labeled with the infrared dye IR-800 (14). Animal imaging after DV treatment demonstrated that IR-800–labeled DV reached and concentrated in the stroke area, while IR-800 dye control was less concentrated and more evenly distributed through the brain, showing only minimal preference for stroke regions (Figure 2E). Of note, IR-800–labeled DV could be detected in the brain as early as 4 hours after i.p. injection (data not shown) and could still be detected up to 72 hours after injection. Finally, heat-inactivated DV was not detected in stroke brain tissue (data not shown), which together with the above data suggest that DV reaches stroke and peri-infarct brain tissue in an active conformation–dependent manner.

DV is neuroprotective, rapidly restores post-stroke motor function, and rescues DV-deficient mice. Preliminary studies were next performed to determine a potential therapeutic window for post-stroke i.p. DV dosing. DV (2 mg/kg, an effective in vivo DV dose used in mouse solid tumor therapy; ref. 14) was administered 2, 4, 8, 12, and 24 hours after stroke, followed by a second dose on PSD 2 and a third dose on PSD 3 (n = 5 WT mice for each time point

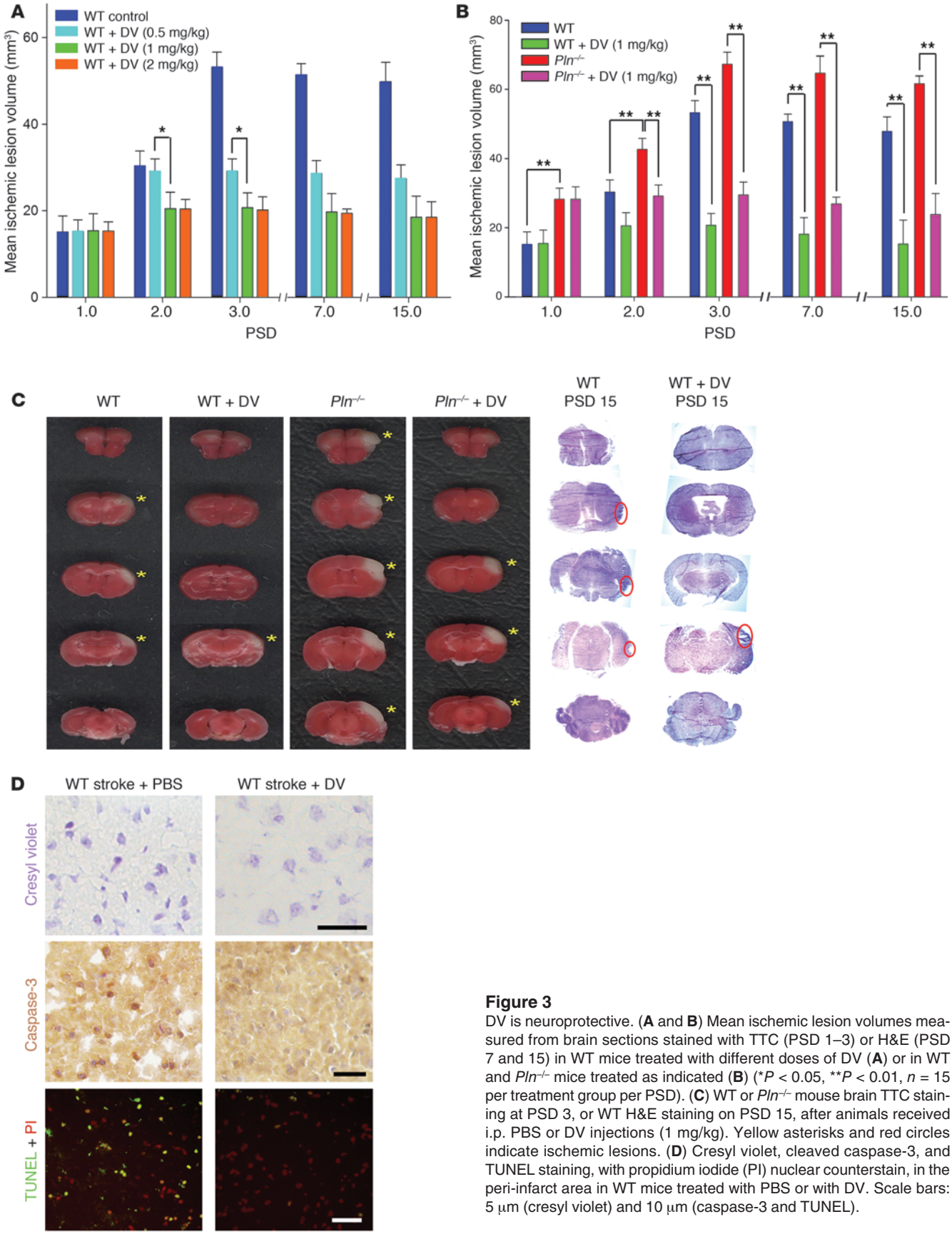

Figure 3

DV is neuroprotective. (**A** and **B**) Mean ischemic lesion volumes measured from brain sections stained with TTC (PSD 1–3) or H&E (PSD 7 and 15) in WT mice treated with different doses of DV (**A**) or in WT and *Pln*$^{-/-}$ mice treated as indicated (**B**) (*$P < 0.05$, **$P < 0.01$, $n = 15$ per treatment group per PSD). (**C**) WT or *Pln*$^{-/-}$ mouse brain TTC staining at PSD 3, or WT H&E staining on PSD 15, after animals received i.p. PBS or DV injections (1 mg/kg). Yellow asterisks and red circles indicate ischemic lesions. (**D**) Cresyl violet, cleaved caspase-3, and TUNEL staining, with propidium iodide (PI) nuclear counterstain, in the peri-infarct area in WT mice treated with PBS or with DV. Scale bars: 5 μm (cresyl violet) and 10 μm (caspase-3 and TUNEL).

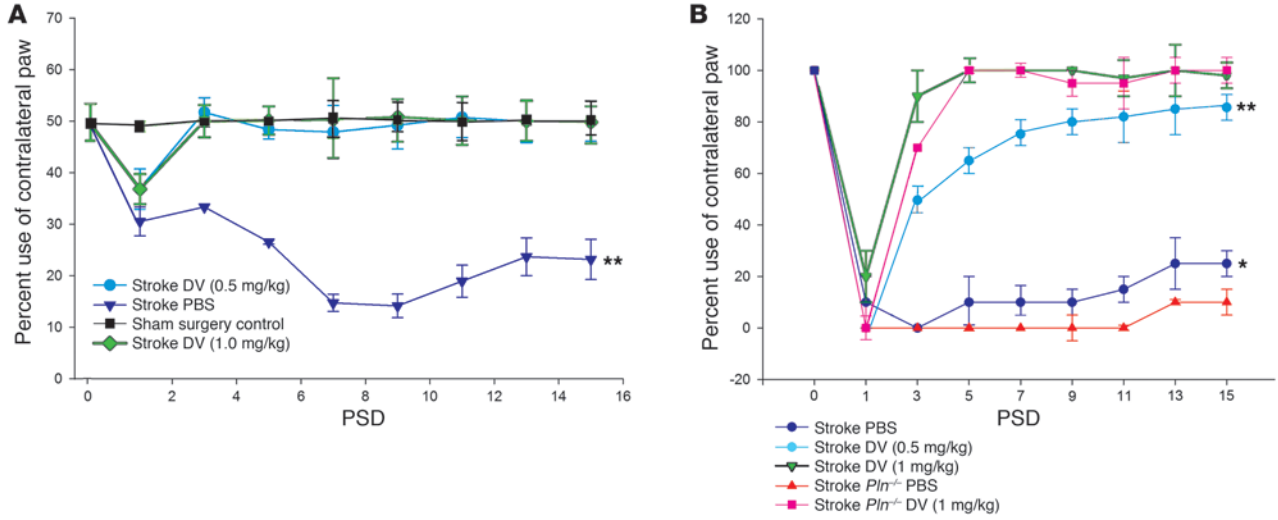

Figure 4
DV restores post-stroke motor function. (**A**) Cylinder test of post-stroke motor function in stroke rats treated as labeled (**$P < 0.01$, all treatment groups compared with PBS control, P = NS between all treatment groups; $n = 15$ per treatment group). (**B**) Vibrissae-elicited forelimb placement test on stroke littermate WT or *Pln*$^{-/-}$ mice treated as labeled. DV-treated (0.5 mg/kg and 1 mg/kg) groups were significantly different from their untreated counterparts (**$P < 0.01$). The DV-treated (0.5 mg/kg) WT mice were significantly different from the DV-treated (1 mg/kg) WT mice ($P < 0.05$). The *Pln*$^{-/-}$ DV-treated mice were significantly different from the WT DV-treated mice (*$P < 0.05$). The WT 1 mg/kg DV group was indistinguishable from the sham surgery control group (P = NS).

of initial DV treatment; mean ischemic lesion size evaluated on PSD 3). Administration of the first dose of DV 2–12 hours after stroke was no more effective in reducing mean ischemic lesion size on PSD 3 than administering the first dose on PSD 2 (data not shown). This result suggests that DV administered 12 hours or less after stroke onset did not affect mean ischemic stroke lesion size. Therefore, for most subsequent experiments, DV was first administered 24 hours after stroke. We next examined the effects of variable doses of DV (0.5, 1, or 2 mg/kg) on PSD 1, 2, 3, 7, and 15 on ischemic stroke lesion volume in WT mice and rats (Figure 3A, mouse data shown). On PSD 1, 8 hours after the first administered doses of DV at all concentrations, heat-inactivated DV, or PBS control, there was no significant difference in mean ischemic lesion volume between the treatment groups. However, by PSD 2, further significant increases in ischemic stroke lesion volume seen in WT stroke mice could be prevented with additional DV (1 and 2 mg/kg) treatment. By PSD 3, the lowest dose of DV tested (0.5 mg/kg) could prevent further increases, but not as much as larger DV doses, demonstrating a DV dose response effect on mean ischemic lesion size. As no differences were noted between the 1-mg/kg and 2-mg/kg doses of DV, we elected to use 1-mg/kg dosing for most subsequent in vivo experiments. DV "replacement therapy" in *Pln*$^{-/-}$ mice had similar effects on mean ischemic stroke volume by PSD 2 (Figure 3, B and C). Further analysis of peri-infarct brain regions from PBS- and DV-treated WT mice on PSD 3 revealed that DV treatment resulted in more neurons with normal morphology, fewer shrunken and misshapen cells, decreased staining of the 17- to 20-kDa caspase-3 cleavage product, and a decreased number TUNEL-positive cells (Figure 3D) (4). Collectively, these results demonstrate that DV treatment is neuroprotective when first administered 24 hours after MCA occlusion.

We next hypothesized that DV's neuroprotection might result in improved post-stroke motor function. When the cylinder test for rats (25) was used, DV treatment significantly increased spontaneous use of the stroke-affected forelimb by PSD 3, which was sustained until PSD 15 (Figure 4A), demonstrating that administered DV persistently restored post-stroke function to pre-stroke levels in rats. Increased doses of DV in post-stroke rats (1–2 mg/kg) had no additional positive post-stroke motor effect (DV 1 mg/kg shown). When the vibrissae-elicited forelimb placement test (26) was used on WT and *Pln*$^{-/-}$ mice (sham surgery also had no effect; data not shown), use of the stroke-affected forelimb in the DV-treated WT groups significantly improved by PSD 3 (DV 1 mg/kg) and PSD 5 (DV 0.5 mg/kg; although this lower dose of DV was overall slightly less effective in improving motor function in mice); stroke forelimb use persisted at this level or further improved (in the case of DV 0.5 mg/kg treatment) through PSD 15, while the PBS-treated mice remained significantly impaired through PSD 15 (Figure 4B). Furthermore, the near complete lack of stroke-affected paw use in *Pln*$^{-/-}$ mice was rescued by DV replacement therapy. The WT DV-treated (1 mg/kg) group was indistinguishable from the sham surgery control group (data not shown) by PSD 5. Finally, increased doses of DV (2 mg/kg) in WT or *Pln*$^{-/-}$ mice had no additional positive post-stroke effect (data not shown). Therefore, in two distinct stroke models in two species, DV treatment persistently (i.e., at least to PSD 15) restored post-stroke motor function to baseline pre-stroke function by PSD 3.

DV neuroprotection involves VEGF and VEGFR. It was next hypothesized that DV could be neuroprotective and restore post-stroke motor function after ischemic stroke by increasing growth factor concentrations. We focused on VEGF for several reasons: DV activity outside of the brain has been linked to the suppression of VEGF signaling (27), perlecan synthesis and release in brain endothelial cells is induced by VEGF (28), and VEGF is known to be neuroprotective (8, 9). We found that total VEGF concentrations following post-stroke DV treatment (as compared with PBS treatment)

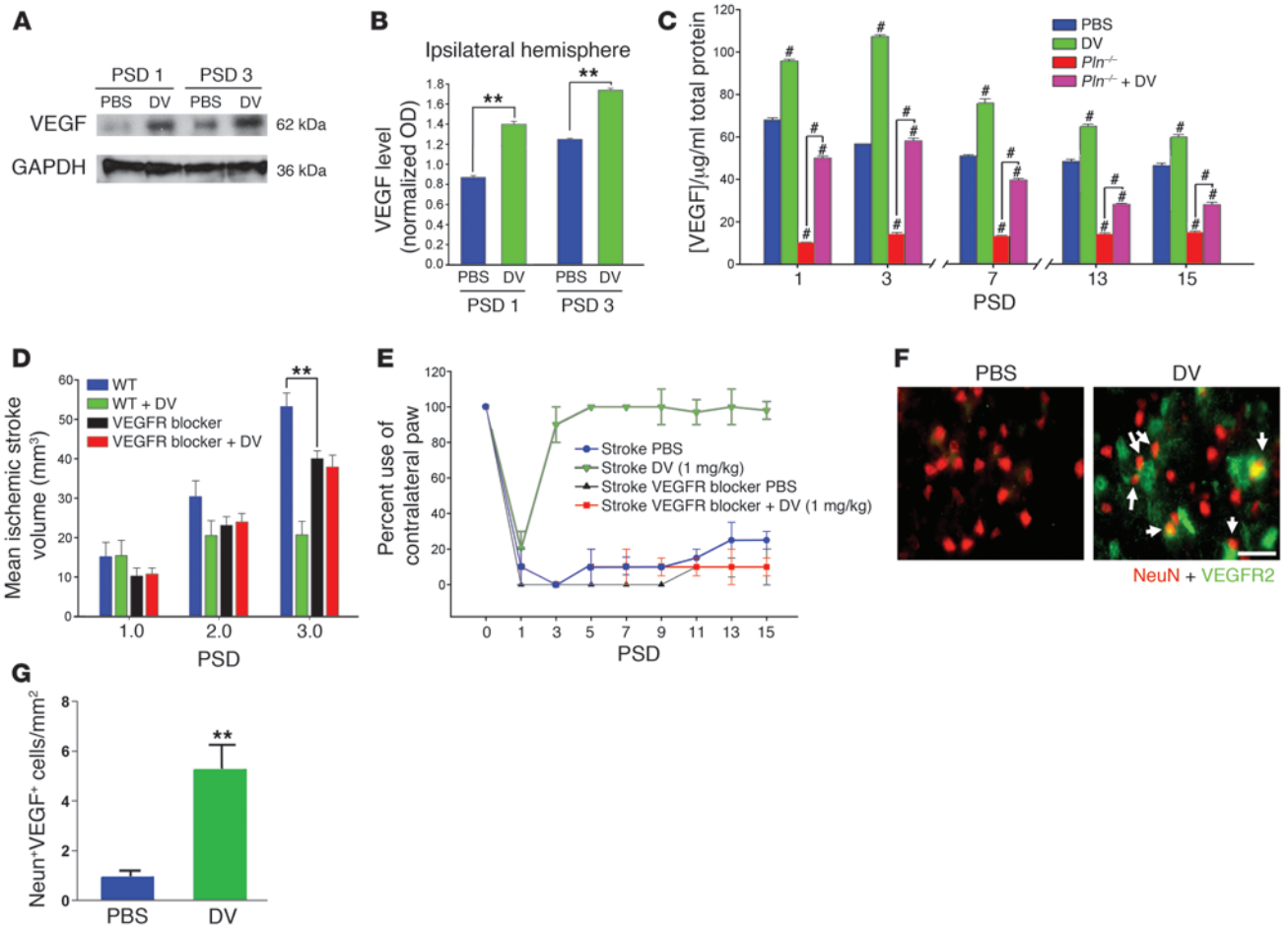

Figure 5

DV neuroprotection is VEGF and VEGFR mediated. (**A**) Anti-VEGF Western blot analysis of ipsilateral stroke hemispheres as labeled, with GAPDH as internal loading control. (**B**) Densitometry analysis of VEGF Western blot as shown in **A** as normalized to corresponding GAPDH bands (**$P < 0.01$, $n = 15$ per treatment group, per PSD). (**C**) Plot of VEGF ELISA ipsilateral stroke brain tissue treated as labeled ($^{\#}P < 0.01$ as compared with corresponding PBS-treated WT control or as labeled, $n = 3$ per treatment group per PSD). (**D**) Mean ischemic lesion volumes of stroke WT mice on PSD 1–3 treated as labeled (**$P < 0.01$, $n = 15$ per treatment group per PSD). (**E**) Vibrissae-elicited forelimb placement test on WT mice treated as labeled. DV had no effect in animals also treated with PTK787/ZK 222584 (P = NS). (**F**) NeuN and VEGFR2 co-immunohistochemistry of PSD 5 peri-infarct brain tissue of mice treated as labeled. White arrows indicate cells that were positive for both NeuN and VEGFR2. Scale bar: 50 μm. (**G**) Number of NeuN- and VEGFR2-positive cells per mm^2 in the peri-infarct regions as labeled (**$P < 0.01$, $n = 10$ images per animal, 5 animals per treatment condition).

significantly increased on PSD 1 and further increased by PSD 3 before gradually diminishing through PSD 15 (Figure 5, A–C). This contrasts with post-stroke VEGF levels in PBS-treated WT mice, which diminished from PSD 1 onward, a result that is consistent with previous observations (29). Interestingly, DV administered prior to 24 hours after stroke (2, 4, 8, or 12 hours) failed to significantly increase stroke brain VEGF levels as measured 8 hours after treatment, or on PSD1 (data not shown). Furthermore, post-stroke *Pln*$^{-/-}$ mouse brains had persistently unchanged and lower levels of VEGF, thus linking the relative absence of endogenous perlecan/DV to diminished post-stroke VEGF production. Finally, this diminished post-stroke VEGF in *Pln*$^{-/-}$ mice could be reversed to near WT levels with post-stroke DV treatment.

Next, experiments were performed in which mice were first pretreated with the VEGFR tyrosine kinase inhibitor PTK787/ZK 222584 (30) or PBS vehicle control prior to stroke and through PSD 15. VEGFR inhibition by itself resulted in significantly smaller mean ischemic lesion volumes by PSD 3 (mean ischemic lesions trended smaller but were not significantly smaller than in PBS-treated controls on PSD 1 or 2) as compared with control PBS treatment (Figure 5D). However, the increase in mean ischemic lesion volume size from PSD 1 to 3 in VEGFR blocker–treated mice could not be prevented with additional DV treatment, further suggesting the involvement of VEGF and VEGFR in DV-mediated neuroprotection. Finally, although VEGFR blockade resulted in overall smaller ischemic lesion volumes than PBS treatment, VEGFR blocker–treated mice exhibited near identical deficits in motor function over 15 days, which could not be improved with additional DV treatment (Figure 5E), linking DV post-stroke motor recovery effects to VEGFR.

It was next hypothesized that if DV were neuroprotective via VEGF, neurons in the peri-infarct area, identified with NeuN

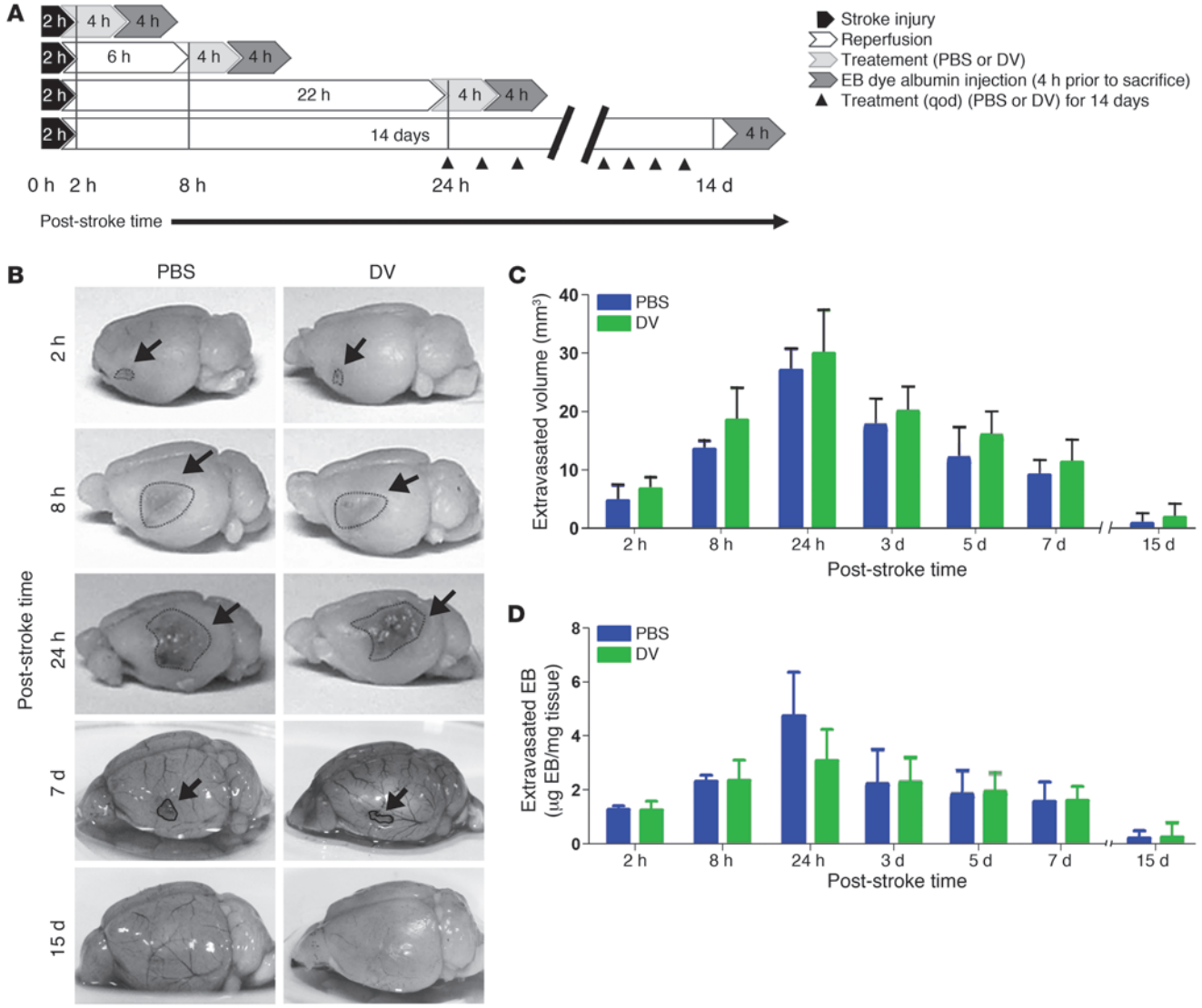

Figure 6

DV does not increase post-stroke blood-brain barrier permeability. (**A**) Schematic of EB-labeled albumin extravasation after stroke in vivo blood-brain permeability paradigm, wherein mice were subjected to stroke and treated with PBS or DV 2, 8, or 24 hours after stroke, followed by i.v. injection of albumin-mixed EB dye (4 hours later), and sacrificed 4 hours later. Alternatively, mice were treated 24 hours after stroke and then every other day with DV or PBS until PSD 14, followed by i.v. injection of albumin-mixed EB dye, and sacrificed 4 hours later. (**B**) Images of brains from mice treated with PBS or DV, per the schematic in **A**, showing the brain surface spread of EB-labeled albumin as circled in black and indicated by the black arrow in each image. (**C**) EB-labeled albumin extravasation volume for the conditions and times of treatment as in **B** (n = 5 per treatment group, per post-stroke time). (**D**) Plot of total EB-labeled albumin (μg) extravasated per mg of brain tissue.

immunohistochemistry, might increase their expression of VEGFR2 with DV treatment. Indeed, a significant increase was noted in VEGFR2 immunoreactivity associated with NeuN-positive cells in the peri-infarct region with DV treatment on PSD 3 (Figure 5, F and G), suggesting that peri-infarct neurons may respond to DV-induced increases in VEGF by increasing their VEGFR2 expression. This further supports the hypothesis that DV could be neuroprotective via VEGF/VEGFR.

DV does not affect post-stroke blood-brain barrier permeability. As VEGF is known to increase blood-brain barrier permeability and edema when administered prior to 24 hours after stroke (7), a potentially serious detrimental side effect of any proposed stroke therapy, potential DV effects on post-stroke blood-brain barrier permeability in vivo were measured by Evan's blue (EB) dye–labeled albumin extravasation, performed as schematized (Figure 6A). No significant change in EB dye–labeled albumin extravasation (quantitatively measured by both volume and concentration of extravasation) was observed in stroke animals treated with DV either prior to or at 24 hours following stroke (the former result was expected due to DV failing to increase stroke VEGF levels when administered prior to 24 hours after stroke), or on PSD 3, 5, 7, or 15 after multiple doses of DV given on PSD 1, 3, 5, 7, 9, 11, 13, and 15 (Figure 6, B–D). Therefore, post-stroke DV administration does not cause further acute or more chronic breakdown of the blood-brain barrier.

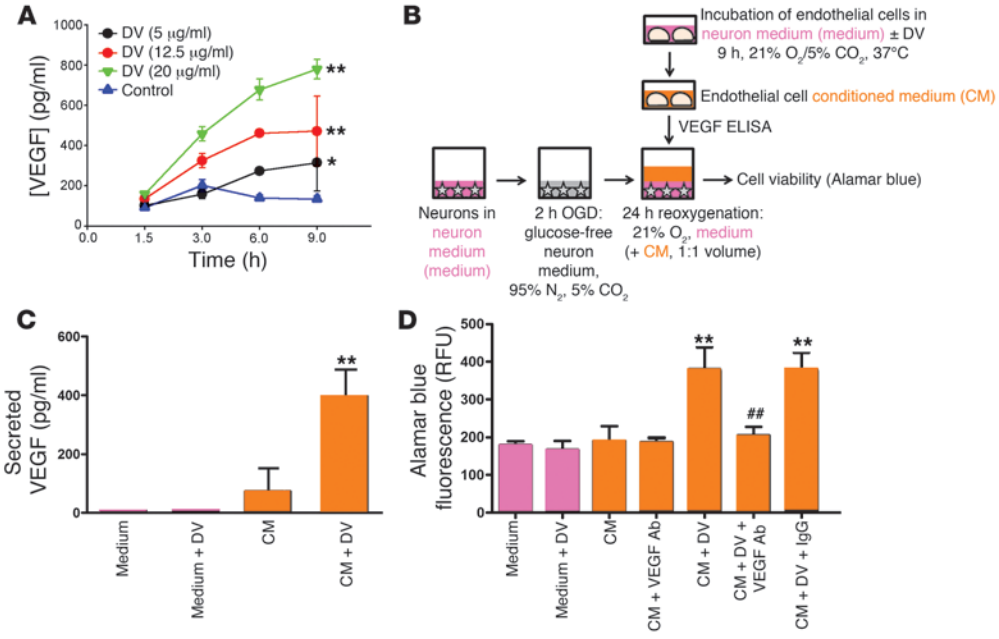

Figure 7

DV is neuroprotective in vitro via enhancement of VEGF secretion from brain endothelial cells. (**A**) VEGF ELISA from conditioned media of mouse brain endothelial cells with different treatment concentrations of DV over time as indicated (*$P < 0.05$, **$P < 0.01$, $n = 15$ per treatment group per time measured). (**B**) Schematic of fetal cortical neuron OGD protocol used in this study. In **B**–**D**: pink, neuron medium (Medium); orange, conditioned medium (CM). (**C**) VEGF ELISA data from fresh neuron medium and CM with or without DV (**$P < 0.01$, $n = 5$ separate experiments, each condition performed in triplicate per experiment). (**D**) Mean Alamar blue fluorescence measurements (excitation wavelength of 560 nm and emission wavelength of 590 nm) of fetal cortical neurons exposed to OGD as outlined in **B** as an indicator of cell viability (**$P < 0.01$ compared with CM alone, ##$P < 0.01$ compared with CM + DV, $n = 5$ separate experiments, each condition performed in triplicate per experiment).

DV increases production and release of VEGF in brain endothelial cells. Based on the above results, the role of VEGF in DV mechanisms was further examined in vitro. First, it was determined that DV treatment increased VEGF production and release in primary cultured brain endothelial cells but not in astrocytes or cortical neurons (Figure 7A; negative results for astrocytes and neurons not shown). Specifically, DV increased *Vegf* mRNA by approximately 8-fold (data not shown). Furthermore, DV significantly increased VEGF release from 3 to 24 hours in a dose-dependent fashion (Figure 7A). To further determine whether the neuroprotective effect of DV could involve endothelial-derived VEGF secretion, we exposed primary mouse cortical neurons to oxygen glucose deprivation (OGD) stress (Figure 7B) in neuronal cell medium, followed by reoxygenation in neuronal medium conditioned by brain endothelial cells (generated by 9 hours of exposure to brain endothelial cells in normoxic conditions with or without DV), with or without additional VEGF neutralizing antibody (or IgG control) added to the cells. Medium conditioned by brain endothelial cells was assayed for VEGF content by ELISA (Figure 7C), which revealed significantly increased VEGF levels only when DV was added during the 9-hour conditioning period. Collectively, our results indicate that direct administration of DV to neurons (in fresh neuronal medium) did not promote their survival. Likewise, conditioned medium from brain endothelial cells (which contained minimal VEGF; Figure 7C) had a minimal effect on post-OGD neuronal survival, while DV-exposed conditioned medium significantly enhanced neuronal survival (Figure 7D). Importantly, the latter effect could be inhibited with VEGF neutralizing antibody, but not by IgG control. These results suggest that DV indirectly protects neurons via enhancement of VEGF release from endothelial cells, rather than via direct effects on neurons.

DV unexpectedly enhances brain angiogenesis in a VEGF- and VEGFR-dependent fashion. Although DV is a known inhibitor of angiogenesis (13), its ability to trigger the synthesis and release of the potently proangiogenic VEGF from brain endothelial cells suggests the possibility that DV could be proangiogenic in the brain. However, as angiogenic brain endothelial cells do not express the previously identified DV receptor $\alpha 2\beta 1$ integrin (refs. 15, 31, and Supplemental Figure 5), DV's exact target in the brain was unpredictable. The potential effect of DV on peri-infarct blood vessel density and angiogenesis was assessed by von Willebrand factor immunohistochemistry and CD31 co-immunohistochemistry with the cell proliferation marker Ki-67, respectively. On PSD 3, blood vessel density unexpectedly increased in peri-infarct regions in WT mice treated with DV, becoming increasingly prominent by PSD 5 and plateauing by PSD 9–15 (Figure 8, A and B). Similar results were obtained in post-stroke rats (data not shown). Furthermore, $Pln^{-/-}$ mice had a profoundly diminished (i.e., less than that of WT mice) post-stroke peri-infarct vascular density from PSD 3 to PSD 15 that could be rescued (and further enhanced beyond the corresponding WT PBS-treated angiogenic response) by DV administration (Figure 8, A and B), further underscoring the importance of endogenously generated DV to the brain's post-stroke response. Likewise, heat-inactivated DV had no effect on post-stroke peri-infarct blood vessel density, as expected (data not shown) (14). Furthermore, pretreatment (i.e., prior to stroke and then every day after stroke) with PTK787/ZK 222584 as above significantly decreased post-stroke peri-infarct vascular density, which could not be overcome by additional DV treatment. Next, Ki-67 and CD31 co-immunohistochemistry was used to determine whether DV was proangiogenic or simply vasculoprotective after stroke. These experiments demonstrated that post-stroke DV increased the density of peri-infarct Ki-67–positive blood vessels on PSD 5 and 7, which diminished to control levels by PSD 13 (Figure 8, C and D). Collectively, these results suggest that DV is an unexpected enhancer of post-stroke angiogenesis.

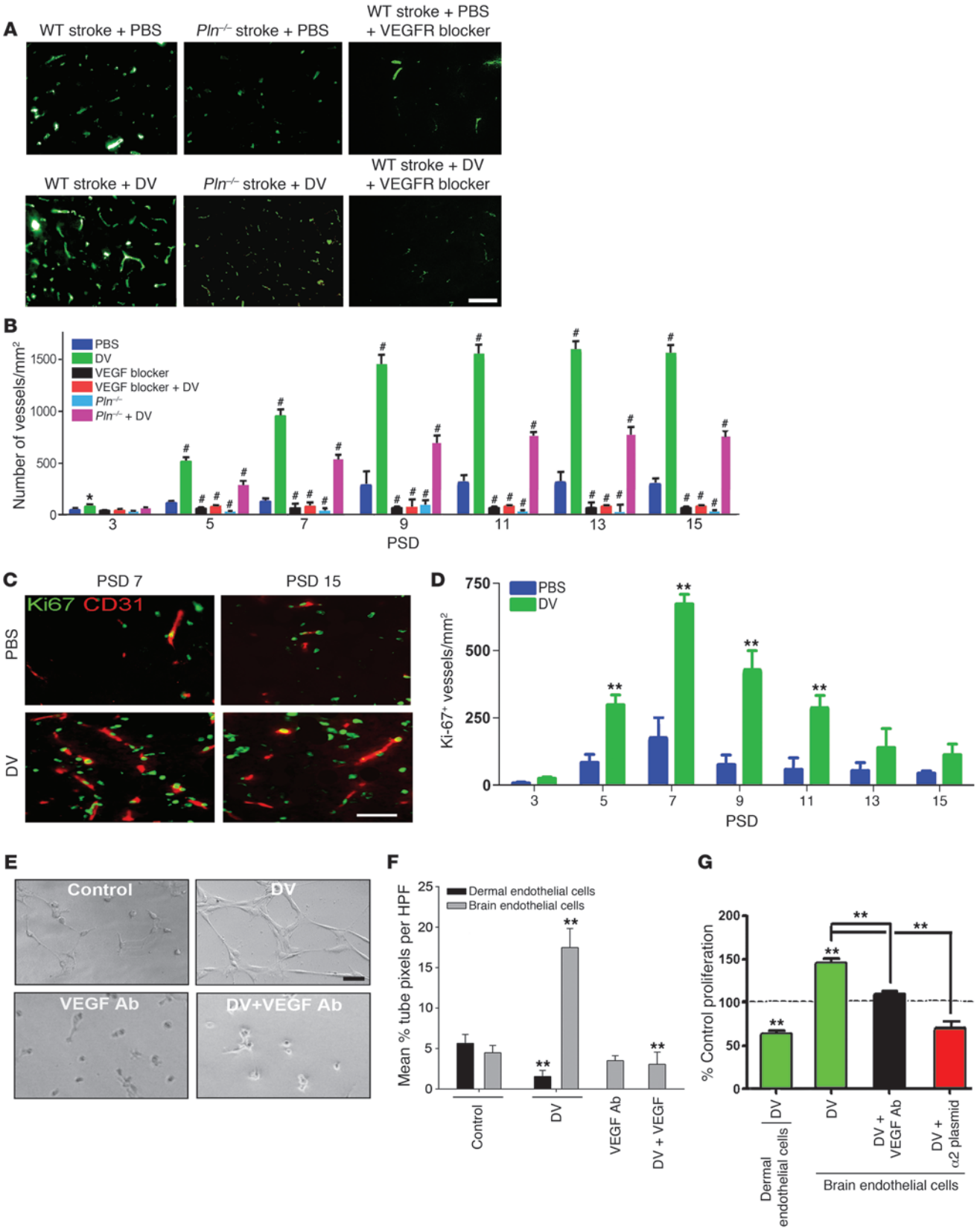
A
WT stroke + PBS
Pln−/− stroke + PBS
WT stroke + PBS + VEGFR blocker
WT stroke + DV
Pln−/− stroke + DV
WT stroke + DV + VEGFR blocker
B
Number of vessels/mm2
PBS
DV
VEGF blocker
VEGF blocker + DV
Pln−/−
Pln−/− + DV
PSD
C
PSD 7
PSD 15
Ki67 CD31
PBS
DV
D
Ki-67+ vessels/mm2
PBS
DV
PSD
E
Control
DV
VEGF Ab
DV+VEGF Ab
F
Mean % tube pixels per HPF
Dermal endothelial cells
Brain endothelial cells
Control
DV
VEGF Ab
DV + VEGF
G
% Control proliferation
Dermal endothelial cells
DV
DV
DV + VEGF Ab
DV + α2 plasmid
Brain endothelial cells

Figure 8
DV increases brain angiogenesis in a VEGF- and VEGFR-dependent fashion. (**A**) Von Willebrand factor immunohistochemistry (green) micrographs of peri-infarct brain on PSD 5 from mice treated as labeled. Scale bar: 10 μm. (**B**) Number of blood vessels/mm^2 (as in **A**) in the peri-infarct region for each treatment group as labeled (*P < 0.05, #P < 0.01 compared with PBS-treated WT, n = 10 images per animal, 5 animals per treatment condition). (**C**) Ki-67 (green) and CD31 (red) co-immunohistochemistry micrographs of peri-infarct brain of WT mice as labeled. Scale bar: 10 μm. (**D**) Number of Ki-67–positive blood vessels (CD31$^+$) in the peri-infarct region of WT mice as labeled (**P < 0.01 compared with PBS-treated WT, n = 10 images per animal, 5 animals per treatment condition). (**E**) Matrigel capillary tube–like structure assay with mouse primary brain endothelial cells treated as labeled. Scale bar: 10 μm. (**F**) Quantification of Matrigel capillary tube assays (as in **E**) (**P < 0.01, n = 15 HPFs per experiment, 5 separate experiments, each condition in triplicate per experiment). (**G**) Proliferation of mouse dermal and brain endothelial cells as labeled after 48 hours in serum-free medium as measured via MTS assay (**P < 0.01, n = 5 separate experiments, each condition performed in triplicate per experiment). Values shown as percent of control proliferation arbitrarily set at 100% for each cell type.

To further examine DV's brain proangiogenic effect, we analyzed the effect of DV on isolated mouse brain microvascular endothelial cells in several stages of angiogenesis, and compared the results with those obtained with DV on mouse dermal microvascular endothelial cells, in which DV has been previously shown to inhibit angiogenesis (13). DV significantly increased brain endothelial cell capillary tube–like structure formation, and this could be significantly inhibited with VEGF neutralizing antibody (Figure 8, E and F), whereas DV significantly inhibited dermal endothelial cell tube formation (Figure 8F). Similarly, DV increased brain endothelial cell proliferation rates by 50% ± 3% compared with control, which could also be inhibited with VEGF neutralizing antibody (Figure 8, E and F). As expected, DV inhibited dermal endothelial cell proliferation. Similar results were obtained with rat and human brain endothelial cells (Supplemental Figure 6). As further evidence that these proangiogenic effects were not due to potential fibronectin contamination, anti-fibronectin antibody had no effect on DV-induced increases in brain endothelial cell proliferation or tube-like structure formation, but did inhibit fibronectin-specific effects (Supplemental Figure 4, D–F). Intriguingly, when these cells were made to express α2β1 integrin (Supplemental Figure 7), DV inhibited rather than enhanced their proliferation (Figure 8G), thereby suggesting that the absence of α2β1 integrin from brain microvascular endothelial cells is essential to DV's proangiogenic effects in the brain. Collectively, these results demonstrate that DV's proangiogenic effects are VEGF- and VEGFR-mediated and that DV's effects on brain endothelial cells are distinct from its effects on non-brain endothelial cells.

DV post-stroke effects are α5β1 integrin mediated. We reasoned that DV-induced VEGF release might be due to both the absence of DV's α2β1 receptor in brain microvascular endothelial cells (refs. 13, 15, and Supplemental Figure 8) and the presence of a distinct DV receptor. We focused on the α5β1 integrin because: (a) perlecan, DV's parent molecule, increases α5β1 integrin expression in brain endothelial cells (32); (b) perlecan supports β1 integrin–mediated cell adhesion via its DV region (33); (c) DV can inhibit cell adhesion to fibronectin (without directly binding to the fibronectin) (34), a primary ligand for α5β1; and (d) α5β1 is downregulated in the mature brain until being reexpressed in brain endothelial cells after hypoxia or stroke, the latter likely taking days to reach maximal levels (32), a post-stroke expression pattern consistent with DV's therapeutic time window/increase in VEGF levels. Furthermore, α5β1 is critical for vascular development (35) and promotes post-stroke brain angiogenesis (32).

To determine the relevance of α5β1 integrin to DV's post-stroke effects, we investigated the potential for DV treatment to increase post-stroke expression of α5β1 integrin. Figure 9A shows that on PSD 3, DV-treated animals expressed more α5 in their stroke hemisphere. Further analysis demonstrated this increase to be most prominent in the peri-infarct vasculature (Figure 9B). Next, stroke WT mice were treated with tail vein injections of α5β1 function blocking antibody (or isotype control IgG) on PSD 1, 2, and 3. α5β1 function blocking antibody (but not control IgG; data not shown) treatment prevented the effects of DV treatment on mean ischemic lesion size on PSD 1, 2, or 3 (Figure 9C), neuroprotection (Figure 9, C and D), functional recovery (Figure 9E), and peri-infarct blood vessel density (Figure 9, F and G). Interestingly, α5β1 function blocking antibody administration resulted in significantly larger mean ischemic lesion volumes (as compared with PBS treatment) by PSD 2–3 and significantly lower post-stroke peri-infarct vascular density by PSD 5–7, the latter result underscoring the importance of α5β1 to brain microvasculature. Finally, treatment with α5β1 function blocking antibody resulted in less detectable VEGF in mouse brains on PSD 1 (as compared with PBS treatment of stroke mice), and levels were unaffected by DV. As before, treatment with control IgG had no effect on VEGF levels (data not shown). Collectively, these experiments suggest that functionally available α5β1 integrin is necessary for DV's post-stroke therapeutic effects and important for post-stroke VEGF release.

DV binds to the α5β1 integrin, causing VEGF production and release. To further investigate the role of α5β1 integrin in DV's effects on brain endothelial cells, we knocked down the α5 integrin subunit with α5 siRNA (75% knockdown achieved; Supplemental Figure 8). Importantly, brain microvascular endothelial cells treated with α5 siRNA remained healthy (data not shown). Brain endothelial cell migration toward DV was inhibited by either α5β1 integrin subunit knockdown or soluble α5β1 protein, which we hypothesized could compete for DV binding with α5β1 localized to the brain endothelial cell surface (Figure 10A). Likewise, the α5β1-specific binding peptide CRRETAWAC (36) or α5 knockdown could inhibit DV's effects on brain endothelial cell capillary tube–like structure formation and proliferation (Figure 10, B and C).

The potential for direct interaction between α5β1 and DV was next confirmed via optical biosensor analysis (Figure 10D). Specifically, DV was determined to bind to α5β1 integrin with K_{on}, K_{off}, and K_d of $3.8 \times 10^6 \pm 2.7 \times 10^5$ $M^{-1}s^{-1}$, $7.2 \times 10^{-1} \pm 1.1 \times 10^{-1}$ s^{-1}, and $1.6 \times 10^{-7} \pm 7.2 \times 10^{-8}$ M, respectively. Also, as the presence of integrin ligand is known to increase that integrin's cellular expression (32), DV was shown to increase α5 mRNA expression 2-fold. Furthermore, α5β1 integrin knockdown prevented DV from increasing VEGF release (Figure 10E). Collectively, these experiments demonstrate that DV binds to, increases the mRNA transcription of, and exerts its proangiogenic effects (in vitro) via α5β1 integrin–mediated VEGF secretion.

Discussion

These studies demonstrate that perlecan DV is persistently generated in the post-stroke rat and mouse brain and is potentially sig-

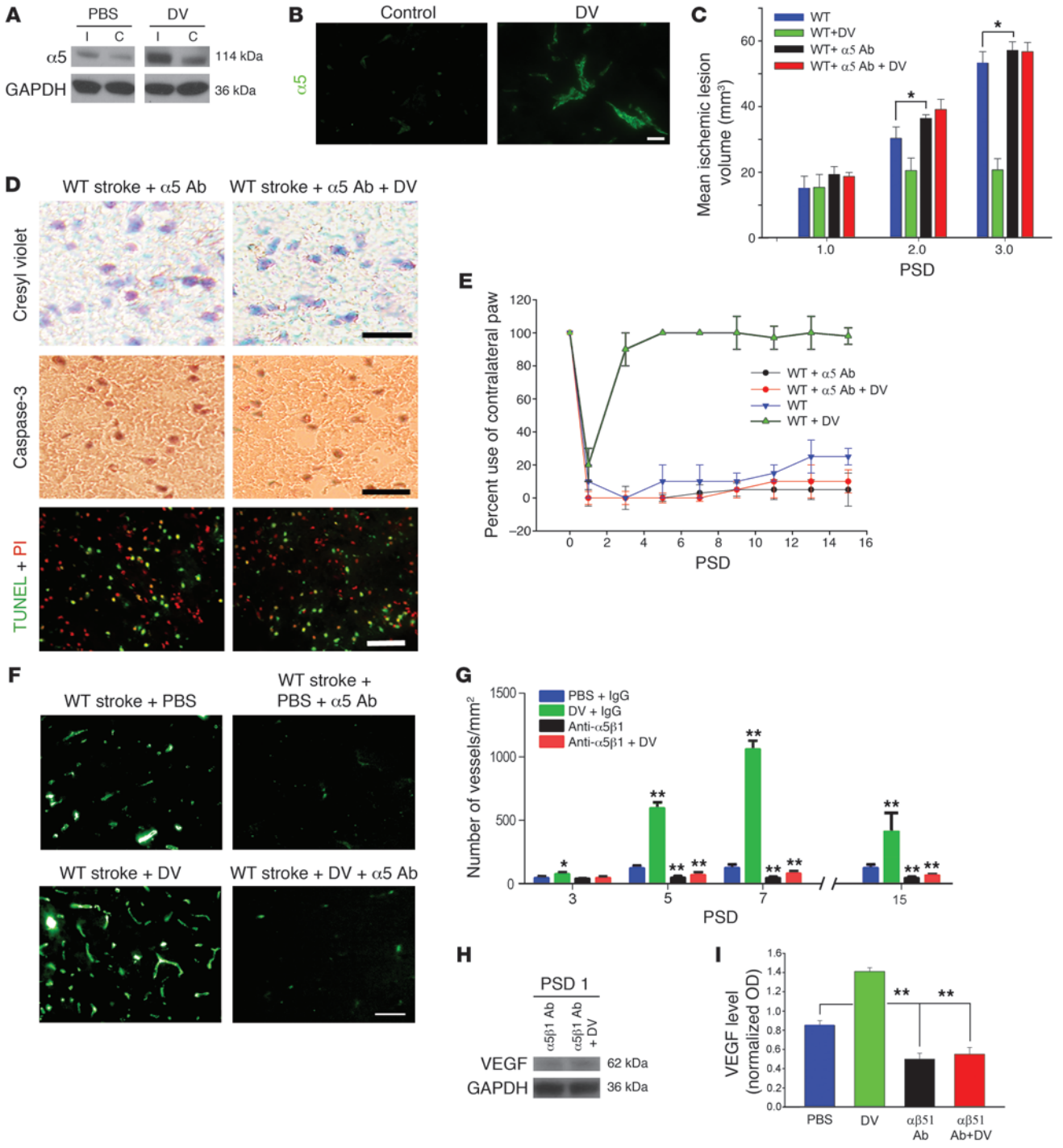

Figure 9

DV effects are mediated via the α5β1 integrin in vivo. (**A**) Anti-α5β1 Western blot analysis from PSD 3 mouse brain tissue treated as labeled, with GAPDH as internal control. (**B**) α5β1 immunohistochemistry of mouse PSD 3 peri-infarct brain tissue with or without DV treatment. Scale bar: 10 μm. (**C**) Quantification of mean ischemic lesion volumes of stroke WT mice on PSD 1–3 as labeled (*$P < 0.05$, $n = 15$ per treatment condition per PSD). (**D**) Cresyl violet staining, caspase-3 17- to 20-kDa cleavage product immunostaining, and TUNEL staining with PI of peri-infarct brain regions as labeled. Scale bars: 10 μm. (**E**) Vibrissae-elicited forelimb placement test on WT mice treated as labeled ($n = 15$ mice per condition from 3 separate experiments with 5 mice each). (**F**) Von Willebrand factor immunohistochemistry (green) on PSD 5 from WT mice treated as labeled. Scale bar: 10 μm. (**G**) Peri-infarct blood vessel quantification as labeled (*$P < 0.05$, **$P < 0.01$ compared with PBS + IgG on the same day, $n = 20$ images analyzed per animal, 10 animals per experimental condition). (**H**) Anti-VEGF Western blot analysis of mouse stroke hemispheres with internal GAPDH as control. (**I**) Optical density quantification of VEGF Western blot analysis as shown in **H** (**$P < 0.01$, $n = 5$ per experimental condition).

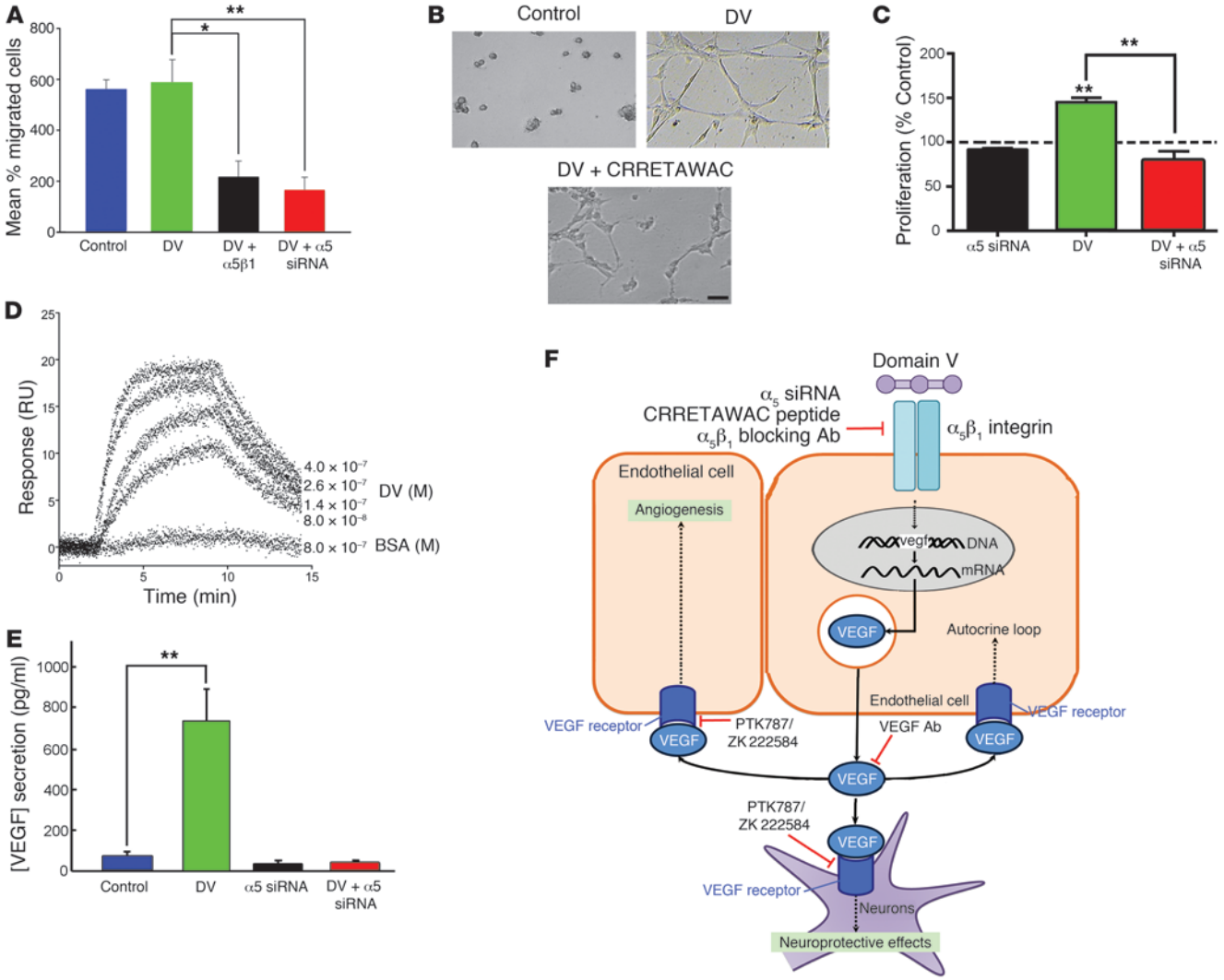

Figure 10

DV's effects are mediated via the α5β1 integrin in vitro. (**A**) Mean percentage of brain endothelial cells (±SD) migrating toward 3% FBS (control) or DV with or without α5β1-GST soluble protein or α5 knockdown with α5 siRNA (as normalized to no chemoattractant negative control) (*P < 0.05, **P < 0.01, n = 5 separate experiments, each condition performed in triplicate per experiment) (**B**) Brain endothelial cells, either untreated or treated with DV or DV plus the α5β1-specific binding peptide CRRETAWAC, on Matrigel after 12 hours. Scale bar: 10 μm (**C**) Quantification of proliferation of brain endothelial cells ± α5 integrin plasmid after 48 hours ± DV measured via MTS assay (n = 15, mean ± SD normalized to control proliferation arbitrarily set to 100%, **P < 0.01, n = 5 separate experiments, each condition performed in triplicate per experiment). (**D**) Optical biosensor traces showing the association and dissociation of DV and BSA (control) with immobilized α5β1integrin at the concentrations (in M) listed; RU, relative units. (**E**) VEGF ELISA data from brain endothelial cell–secreted medium treated as labeled (**P < 0.01. n = 5 separate experiments, each condition performed in triplicate per experiment). (**F**) Schematic for DV-induced VEGF production and release in brain microvascular endothelial cells via α5β1 integrin. Inhibitors used in this study are indicated with red lines. The various proposed effects of VEGF (i.e., stimulation of angiogenesis and neuroprotection) are also schematically illustrated.

nificant inasmuch as perlecan/DV-deficient mice experience larger ischemic stroke lesions than their WT littermates. Furthermore, when human recombinant DV was systemically administered 24 hours after stroke, in an effort to augment endogenous DV post-stroke function, it could be detected at and around the site of brain injury by live in vivo animal imaging, and it appeared to deposit in a perivascular distribution in stroke and peri-infarct brain tissue by immunohistochemistry.

DV treatment, in a dose-dependent fashion, prevented volumetric expansion of the ischemic stroke lesion, seen in untreated WT control and *Pln*$^{-/-}$ stroke animals (a "rescue" with "replacement" DV), from PSD 1 to 3. It is worth noting that in both our endothelin-1 and tandem ipsilateral CCA and MCA stroke models, we noted a prominent expansion (i.e., more than 10%–15%) in mean ischemic lesion size from PSD 1 to PSD 3 in WT animals. While not commonly reported, this sort of ischemic lesion expansion has been noted with the endothelin-1 stroke model (37) and other transient CCA and MCA transient occlusion models (38). In the latter, the evolution of ischemic lesion volume is largely dependent on the duration of transient ischemia: 30 minutes of ischemia may

yield a lesion that does not appear until PSD 3, while 90 minutes of ischemia yields a visible infarct on PSD 1 that increases only slightly by PSD 3. In our tandem ipsilateral CCA and MCA occlusion model, ischemia lasted for 60 minutes, an in-between duration that could explain our observation of a visible infarct at PSD 1 that expanded significantly by PSD 3.

DV neuroprotection correlated with recovery of motor function to pre-stroke levels that persisted to at least PSD 15. Interestingly, in motor function testing, DV dose response effects varied slightly between rats, in which 0.5, 1, and 2 mg/kg DV were all equally effective, and mice, in which 0.5 mg/kg was somewhat less effective than 1 and 2 mg/kg of DV. There could be a number of reasons for this, including differences in the absolute amount of DV given to the mice and rats (rats weigh much more than mice, such that 0.5 mg/kg of DV is much more total DV in a rat than a mouse); differences in the stroke models used in each species; differences in the sensitivity to injury between the vibrissae-elicited paw placement test and the cylinder test used in mice and rats, respectively; or slight differences in the amino acid sequence identity between human and rat DV (92%) and human and mouse DV (91%). Additionally, DV, an antiangiogenic protein, unexpectedly enhanced post-stroke brain angiogenesis. Finally, DV was demonstrated to act through a mechanism involving the α5β1 integrin and ultimately increased VEGF production and release in brain endothelial cells.

Perlecan, synthesized and secreted by neurons, astrocytes, and endothelial cells (39), induced in the latter by VEGF (28), is the most sensitive and rapidly processed matrix component after stroke (11). Perlecan proteolysis by cathepsin L occurs within 2 hours of the occlusion of the MCA in nonhuman primates and persists for several days (11). The sustained processing of perlecan and release of DV after stroke are consistent with studies demonstrating an increase in perlecan production in neurons and astrocytes after brain injury (39). In the present study, we have detected an acute, perivascular increase in endogenous perlecan DV levels that gradually plateaued at an elevated level over the course of 7 days after stroke, a temporal pattern that correlates well with the nonhuman primate post-stroke perlecan proteolysis profile (11). This expression profile differs from that of other matrix-derived bioactive fragments such as endostatin (transiently generated after ischemic stroke; ref. 40), underscoring DV's potential for both acute and chronic post-stroke effects.

Having demonstrated that DV is a perivascular product of stroke brain injury, we next determined that post-stroke perlecan/DV deficiency resulted in larger stroke ischemic lesions (which could not be attributed to cerebrovascular anatomical differences in territories vascularized by MCA collateral branches), suggesting that post-stroke perivascular generated DV could play a role in the brain's response to stroke. It is important to note that *Pln*$^{-/-}$ mice had larger infarcts than WT littermate controls at 24 hours of reperfusion, although we found that the exogenous administration of DV prior to 24-hour reperfusion had no effect on ischemic lesion size, suggesting that a deficiency in DV should not impact ischemic lesion size at this time. However, these mice are deficient in the production of all of perlecan (including but not limited to DV), suggesting the possibility that other parts of perlecan besides DV may also play a role in the brain's response to stroke and contribute to the larger infarct seen at 24 hours of reperfusion. For example, as the heparan sulfate chains of perlecan specifically bind FGF2 (41), which has been implicated in reducing infarct volume in animal models of focal cerebral ischemia (42), a perlecan deficiency could possibly result in less FGF2 being present where perlecan is normally expressed in the vascular basement membrane, thereby potentially contributing to larger infarcts at 24 hours of reperfusion. Importantly, however, the ability of exogenous DV replacement therapy to rescue this *Pln*$^{-/-}$ stroke phenotype from PSD 2 onward underscores the relatively significant contribution of DV deficiency to the *Pln*$^{-/-}$ stroke phenotype.

We then reasoned that exogenously administered human recombinant DV could reach and interact with this same stroke and peri-infarct vasculature (after experimental reperfusion in our transient focal ischemia models). Indeed, whole animal imaging of fluorescent dye–labeled DV and immunohistochemistry demonstrated that systemically administered DV reached the infarct and peri-infarct vasculature. While it is unclear whether administered DV crossed the stroke-disrupted blood-brain barrier (a phenomenon that has been described for proteins as large as 2 MDa after stroke; refs. 43, 44), its ability to do so may not be critical to its proposed therapeutic mechanism of action, i.e., interaction with brain endothelial α5β1 integrin.

In this study, we noted a rapid (by PSD 3) functional/motor improvement when DV was first administered 24 hours after stroke. This correlated with neuroprotection, increased total stroke brain VEGF levels, and increased VEGFR2 expression in peri-infarct neurons. Furthermore, VEGFR blockade with PTK787/ZK 222584 prevented these DV effects. Additionally, *Pln*$^{-/-}$ mice generated significantly and persistently less post-stroke VEGF (linking an endogenous decrease in perlecan/DV levels with a decrease in post-stroke VEGF production), which was increased with DV administration. Collectively, these studies link DV to post-stroke VEGF production and suggest that DV-mediated neuroprotection and motor function recovery could be mediated, at least in part, by VEGF. Further in vitro analysis demonstrated that brain endothelial cells are the likely source of DV-induced VEGF production and release. Specifically, we showed that DV could increase *Vegf* mRNA levels and VEGF release in a dose-dependent fashion. As VEGF regulates perlecan synthesis in these cells (45), it is tempting to speculate that DV-induced VEGF release could result in a positive feedback loop that increases perlecan synthesis, which in turn provides more "raw material" for the sustained generation of DV.

Importantly, unlike VEGF administered acutely (i.e., prior to 24 hours) after stroke, acutely administered DV (2 or 8 hours after stroke) did not cause changes in post-stroke edema (see Methods for a description of how this was measured) or increase blood-brain barrier permeability in post-stroke mice. Likewise, in preliminary studies we noted that administration of the first dose of DV 2–12 hours after stroke was no more effective in reducing mean ischemic lesion size than administering the first dose on PSD 2. One possible explanation for these observations is that DV, the activity of which is dependent on increased α5β1 integrin expression in newly stroke-activated brain microvasculature, may be less active/inactive if brain endothelial cell α5β1 integrin levels are minimal, i.e., prior to 24 hours after stroke in rodent models, as is suggested by rodent hypoxia studies (32). Importantly, although relatively few drugs have been shown to be neuroprotective (decrease infarction) when first administered 24 hours after reperfusion, this has been reported for a number of compounds including VEGF (9) and the purinergic ligand 2MeSADP (46), the former reinforcing DV's delayed neuroprotection potential via VEGF-driven mechanisms. The exact therapeutic window for post-stroke DV admin-

istration is also presumably affected by the amount of time it takes for administered DV to reach the brain, which we observed to be approximately 4 hours for i.p. administration, but would be presumably shorter for i.v. administered DV (the efficacy of i.v. administered DV in stroke is currently under investigation). Additionally, a later post-stroke time window could present other advantages for DV stroke therapy. In addition to 24 hours after stroke being a potentially easier "real-world" target for hospitals to achieve than the 3- to 4.5-hour post-stroke target for TPA administration, it is conceivable that immediate co-administration of DV and TPA could result in DV degradation/loss of function by TPA, which could be avoided by DV being administered at least 24 hours after TPA administration, well past the 1-hour action of TPA at the blood clot site. However, despite these potential caveats for DV stroke therapy, DV has other potential therapeutic advantages: it is well tolerated and lacks VEGF's significant systemic hemodynamic side effects (47).

In addition to being neuroprotective, DV also induced an unexpected, albeit modest increase in peri-infarct angiogenesis by PSD 3 that further significantly increased by PSD 7, then diminished to control levels by PSD 15. It is unlikely that this fledgling enhanced angiogenic repair response could significantly account for the PSD 3 motor function recovery noted in this study. Importantly, as described above, this transient increase in post-stroke angiogenesis did not result in increased peri-infarct blood-brain barrier disruption. This could suggest either that these transiently increased new blood vessels are not "leaky" or that they are not actively supporting blood flow, as has been demonstrated for angiogenic PSD 7 peri-infarct blood vessels in C57BL/6 mice by Ohab and colleagues (4). Interestingly, it is these nonperfused blood vessels that reportedly support doublecortin-positive neuroblast migration toward the infarct in a peri-infarct neurovascular niche (4). Indeed, our preliminary observations suggest that DV treatment results in an increase in the number of doublecortin-positive neuroblasts in association with these peri-infarct angiogenic blood vessels on PSD 5 and 7. As VEGF can support such post-stroke neuroblast migration (8), the possibility of VEGF-driven DV effects on post-stroke neuroblast migration and their potential consequences for long-term stroke recovery are actively being investigated.

The ability of the antiangiogenic DV to promote angiogenesis in the cerebral vascular bed following stroke is remarkable. This unexpected result may be due to endothelial heterogeneity, whereby endothelial cells from various sources, with attendant varying microenvironments, receptors, or signal transduction components, respond differently to the same angiomodulatory factors. For example, Wnt/β-catenin signaling is required for CNS, but not non-CNS, angiogenesis (48), and proangiogenic sphingosine-1-phosphate (S1P) is antiangiogenic in brain endothelial cells (49).

Post-ischemic, angiogenic brain endothelia express developmental integrins including α5β1, αvβ5, and αvβ3 (50), of which α5β1 and αvβ3 have been linked to VEGF secretion (51). We were able to experimentally rule out any interaction between DV and αvβ3 (data not shown) but did demonstrate that DV binds to brain endothelial cell α5β1 integrin, resulting in the increased production and release of VEGF. Importantly, when α5β1 was blocked after stroke, total VEGF levels were diminished, an observation that further links post-stroke α5β1 functionality to VEGF release. α5β1 integrin promotes post-stroke brain angiogenesis (32) largely via interaction with its primary ligand, fibronectin (K_d around 1.5 nM), which is also significantly upregulated after hypoxic brain injury (32). The enhanced post-stroke regional expression of α5β1 integrin over time might also explain DV's ability to reach stroke and peri-infarct cortex vasculature, just as α2β1 expression in tumor vasculature supported DV targeting in vivo (14). The rapid post-stroke generation of DV may also help increase α5β1 integrin expression, as supported by our observation that DV increased α5β1 integrin mRNA levels in brain endothelial cells in vitro and α5β1 integrin levels in post-stroke brain tissue.

As DV's affinity for α5β1 (K_d of 160 nM) is many fold less than fibronectin's, one could question how DV might function in an already fibronectin-rich environment. We hypothesized that this could occur if DV binds to α5β1 differently from fibronectin, as has been demonstrated for DV and collagen I binding to α2β1 integrin (27, 31). Supplemental Figure 9 demonstrates that soluble, but not insoluble, DV is capable of increasing brain endothelial proliferation, even in the presence of fibronectin, a scenario that mimics the post-stroke fibronectin-rich in vivo environment. However, fibronectin could enhance cell growth whether soluble or insoluble, suggesting that while DV can function in a fibronectin-rich environment, it may interact differently with brain endothelial cells and α5β1 than fibronectin. Furthermore, as most other endothelial cells express α2β1 and α5β1 integrin, an additional question is, why is DV antiangiogenic in these α2β1/α5β1-coexpressing cells? The answer could lie in DV's varying affinity for each receptor. Bix et al have previously demonstrated that DV binds to α2β1 with a K_d of 80 nM (13), exactly twice the K_d for α5β1 and DV demonstrated in this article. Therefore, in the presence of both receptors, DV may have a binding preference for α2β1 and the antiangiogenic response predominates, as we demonstrated with brain endothelial cells genetically modified to express α2β1 integrin. Finally, it is important to note that human and mouse, and human and rat α5β1 integrin are highly conserved at the amino acid level (91% and 90% identical, respectively, based on GenBank reference sequences NP_002196.2, AAH50943.1, and NP_001101588.1 for human, mouse, and rat, respectively), which would seemingly help account for our human recombinant DV's ability to interact with α5β1 from all 3 species.

A number of recent studies have demonstrated that improving neuroprotection or post-stroke angiogenesis can improve stroke outcome. These experimental therapies include pharmacological agents, growth factors, and stem cell therapies. We now propose a fourth type of stroke therapy, the extracellular matrix fragment perlecan DV, which is persistently generated by the post-stroke brain; reaches the area of injury when systemically administered 24 hours after stroke; is seemingly well tolerated; and, via newly determined cell receptor interactions and growth factor release, is neuroprotective, significantly improves stroke-affected motor function, and (unexpectedly) increases the post-stroke angiogenic response.

Methods

Cell culture. Human brain microvascular endothelial cells (Lonza and Cell Systems), mouse and rat brain microvascular endothelial cells (provided by Jane Welsh, Texas A&M University) were passaged as per the supplier's instructions or as previously described (13). Primary mouse dermal endothelial cells (Celprogen Inc.) were maintained initially as recommended by the manufacturer. After the second passage, cells were passaged to flasks precoated with 1 mg/ml gelatin and fed with culture medium prepared as described previously (52). In all endothelial cells, the presence of endothelial cell markers von Willebrand factor and VEGFR was confirmed via immunohistochemistry and Western blot analysis.

DV protein production. Human DV was cloned into the vector pSecTag2A (Invitrogen) using the primers 5′ DV Asci pSecTag2A: 5′-AGGGCGCGCCATCAAGATCACCTTCCGGC-3′; 3′ DV Xho1 pSEcTag2A: 5′-AGCTCGAGCCGAGGGGCAGGGGCGTGTGTTG-3′. To further confirm that DV effects were not due to any single clone-specific irregularities, we also cloned DV into the vector pCepPu (provided by Maurizio Mongiat, Center for Cancer Research, Aviano, Italy) using the following primers: NHEI whole DV forward 5′-AGGCTAGCGATCAAGATCACCTTCCGGC-3′; XHOI HIS DV reverse 5′-AGCTCGAGCATGATGATGATGATGATGCGAGG-3′. The DV cDNA was amplified from HUVEC cDNA using a GC-rich PCR system and dNTPack (Roche Applied Science). Maxi-preps of DV DNA were transfected into 293FT (for pSecTag2A vector, ATCC) or 293 EBNA (for pCepPu vector) cells via Lipofectamine (Invitrogen). After transfection, the 293 cells were put into a CELLine Adhere 1000 bioreactor (Argos Technologies) and grown for 7 days in complete medium containing 10% FBS, 1× antibiotic/antimycotic, 1% G418 sulfate, and 0.05 μg puromycin. After 7 days the complete medium was removed; the cells were washed 5 times to remove any serum with CD293 medium containing 4 mM L-glutamine, 1× antibiotic/antimycotic, 1% G418 sulfate, and 0.05 μg puromycin; and then fresh CD293 medium was added to the cells. The cells were incubated for 7 days, followed by collection of the DV-containing conditioned medium, and DV purification via its C-terminal 6XHis tag and Ni-ATA agarose beads (QIAGEN) as per the company's instructions. Eluted fractions that contained DV were combined and dialyzed against 1× PBS, and the purity of the resultant DV was confirmed via SDS-PAGE stained with Brilliant Blue G Colloidal, silver stain (FASTsilver Gel Staining Kit, Calbiochem) following the manufacturer's instructions, Western blot analysis using commercially available anti-DV antibody (R&D Systems), anti-His antibody (EMD Chemicals) (Supplemental Figure 3) and anti-fibronectin antibody (Abcam) to check for fibronectin contamination of DV preparations. Previously demonstrated antiangiogenic concentrations of DV (250 nM) (13) and heat-inactivated controls (100°C for 30 minutes) were used for all experiments unless otherwise stated.

In vivo stroke models. Adult male Harlan Sprague-Dawley rats, adult (3-month-old male) C57BL/6 WT littermate control mice (mean weight, 26.5 ± 0.5 g), and *Pln*$^{-/-}$ mice expressing 10% of normal amounts of perlecan (in a C57BL/6 background; mean weight, 23.0 ± 0.7 g, an approximate 15% decrease compared with WT littermate controls, as expected; ref. 19) (provided by Kathryn Rodgers, University of Pennsylvania, Philadelphia, Pennsylvania, USA; ref. 19) were subject to transient MCA occlusion by stereotaxic injection with endothelin-1 (American Peptide Co.) or by tandem CCA and MCA transient (ischemia lasted for 60 minutes) occlusion (16, 53), respectively, in accordance with Texas A&M College of Medicine guidelines. Diminished blood flow and subsequent restoration of blood flow were confirmed with a Laser Doppler Perfusion Monitor (PF5010, Perimed) (54), and only those animals that displayed a cerebral perfusion reading less than 10 (approximately 12%–15% of the initial value) on the LDF scale (expressing relative values of cerebral perfusion) and demonstrated reperfusion to within 90% of the initial value were included in subsequent experimentation. Animal physiologic measurements before and after DV injection (1 mg/kg) were made with the MouseOx (STARR Life Sciences Corp.). On PSD 1, blood was collected before and 2 hours after the DV injection (1 mg/kg) for blood gas and ion analysis (IRMA TruPoint blood analysis system) done within 30 minutes after the samples were collected.

The animals were sacrificed up to 15 days after surgery, and brain tissue was removed for analysis. For immunohistochemistry, freshly frozen brain tissue was sectioned via cryostat, fixed with acetone, and stained with antibodies directed to von Willebrand factor (Dako), caspase-3 (Abcam), CD31 and Ki-67 (to assess angiogenic blood vessels, which were identified as both CD31 and Ki-67 positive by co-immunohistochemistry; Santa Cruz Biotechnology Inc.), DV (R&D Systems and Santa Cruz Biotechnology Inc.), perlecan DIV (to distinguish free DV from perlecan-attached DV when used in co-immunohistochemistry with DV antibody; Santa Cruz Biotechnology Inc.), His (Calbiochem), NeuN (Abcam), α5β1 (Millipore), and VEGFR2 (Cell Signaling Technology). In some experiments, the cells (per mm^2) in the peri-infarct area that were both NeuN$^+$ and VEGFR2$^+$ (via co-immunohistochemistry) were manually counted under fluorescence microscopy. Some tissue sections were analyzed by routine TUNEL staining according to the manufacturer's instructions. For immunohistochemistry and TUNEL staining, the site of ischemic injury was identified morphologically. The peri-infarct region of focus was defined as a 500-μm boundary extending from the edge of the infarct core, medial and lateral to the infarct (4). To detect the post-stroke distribution of administered DV, we performed anti-His immunohistochemistry with the appropriate Texas red–conjugated secondary antibody, and whole brain section images were obtained with an Olympus MVX10 microscope. For other immunohistochemistry, images were obtained with a BD Carv II spinning disk confocal imager mounted on a Zeiss Axioplan. The images were captured and analyzed using an attached Apple Macintosh computer and iVision-Mac Image Acquisition and Analysis Software. To confirm stroke size and location, we sectioned and analyzed several animals' brains by 2,3 triphenyltetrazolium chloride (TTC) staining (55) on PSD 1, 2, and 3 or by H&E staining on PSD 7 and 15. For H&E staining, representative 10-μm sections were obtained as for immunohistochemistry from the same brain regions as used for TTC staining. Animals were treated by an investigator who was blinded to the identity of the different treatment groups with i.p. injections of sterile filtered DV (0.5, 1, and 2 mg/kg), heat-inactivated DV control, or PBS vehicle control either on PSD 1, 2, and 3 or on PSD 1, 3, 5, 7, 9, 11, 13, and 15. In some experiments, WT mice were treated with i.v. injections of α5β1 integrin function blocking antibody or IgG control (4 mg/kg) prior to each DV treatment. In other experiments, mice were also treated with the VEGFR inhibitor PTK787/ZK 222584 (2 mg/kg, Selleck Chemicals) or PBS vehicle control by oral gavage, starting 1 day prior to the stroke daily through PSD 15. For each TTC-stained 2-mm sectioned brain (5 sections per brain), ischemic lesion volume was measured with Invision software for Apple Macintosh. Edema was calculated by determining the difference between left hemisphere volume and right hemisphere volume.

MCA-ACA anastomosis analysis. Prior to use in our tandem CCA and MCA occlusion model, the anastomoses between the MCA and ACA in littermate WT and *Pln*$^{-/-}$ were analyzed according to the methods of Maeda et al. (22, 23). ACA-MCA anastomosis points on the brain's dorsal surface were visually identified as defined by Maeda et al. as the narrowest part of the vessel or halfway between the nearest branching points of the ACA and MCA branches, respectively. Adjacent anastomosis points were connected by the line of anastomoses, and the distance from the midline to the line of anastomoses was measured using iVision-Mac Image Acquisition and Analysis Software (BioVision Technologies) on images taken from the dorsal brain surface at coronal planes 2, 4, and 6 mm from the frontal pole (22).

Pre- and post stroke motor function assays. Stroke or sham surgery control rats were placed in a 20 cm (diameter) × 35 cm (height) transparent cylinder for 3 minutes to test limb preference and their ability to support weight on either forelimb (25). As the animal reared to explore the environment, the bilateral, ipsilateral (left), or contralateral (right) paw placements were counted and analyzed by an investigator blinded to the different treatment groups. The percent of contralateral limb use was calculated using the following formula: contralateral contacts/(ipsilateral + contralateral) × 100. Stroke or sham surgery control WT or *Pln*$^{-/-}$ mice were tested with the vibrissae-elicited forelimb placement test (stimulation of the vibrissae triggers reflex extension of the ipsilateral paw in neurologically intact animals) (26) to measure post-stroke motor function. Briefly, the animals

were held by their torsos with the forelimbs hanging freely, and the forelimb placement was induced by gently touching the respective vibrissae against the edge of a Plexiglas plate (size: 4 × 6 inches, 3 inches raised from the bottom). Contralateral and ipsilateral forelimb placement responses were counted, with 10 trials for each side. Placement of each paw on the glass plate in response to the respective vibrissae stimulation was given a score of 1. The proportion of successful placements with the affected forelimb was calculated and converted to percent usage.

In vivo animal imaging of IR-800 dye–labeled DV. DV was labeled with IRDye 800CW dye (Licor Biosciences) as previously described (14). Briefly, 100 μg DV was incubated with 1.5 μl of dye and incubated for 2 hours at room temperature. Conjugated DV was then purified from free dye via Zeba Spin Desalting Columns (Thermo Scientific). Protein concentration was determined by Bio-Rad Protein Assay. The carboxylate form of IRDye 800CW was used as the dye-only control.

DV–IR-800– or IR-800 control–injected animals were imaged at different time points after injection (4 hours to 3 days) using a Kodak In Vivo FX small animal imager. Prior to imaging, animals were anesthetized as per Texas A&M College of Medicine guidelines. Excitation wavelength of 720 nm and emission wavelength of 790 nm were utilized. Images were analyzed using Kodak Molecular Imaging Software and processed with Adobe Photoshop CS.

In vitro angiogenesis assays. Matrigel experiments were performed as previously described (31). After 12–18 hours, cells were imaged and tube formation was quantified (tube pixels/high-power field, 10 areas per condition) with Adobe Photoshop CS. Cell migration was assessed with a modified Boyden chamber (NeuroProbe) following the instructions of the manufacturer. Migration across a type I collagen–coated polycarbonate membrane (PVD-free 8-μm pore) toward VEGF (20 ng/ml), 3% FBS, or DV (300 nm) was assessed after 6–8 hours. Proliferation was assessed after 48 hours in serum-free medium containing 20 ng/ml VEGF with MTS solution (Promega) following the manufacturer's instructions. In some experiments, cells were pretreated with α5β1-specific peptide CRRETAWAC or CRRETADAC control peptide (10 mg/ml, provided by Martin Humphries, University of Manchester, Manchester, United Kingdom) (36).

α5β1 integrin knockdown. Brain microvascular endothelial cells were treated with α5 siRNA (Mission siRNA; Sigma-Aldrich) containing medium with Lipofectamine 2000 (Invitrogen). After 2 hours, this was replaced with antibiotic-free growth medium (M199, 10% FBS, 150 mg/ml bovine brain extract, 60 mg/ml heparin), and cells were allowed to recover overnight. α5 integrin knockdown was confirmed by α5 quantitative PCR and α5 Western blot analysis.

α2 integrin expression. Brain microvascular endothelial cells were transfected with a plasmid vector (pEGFP-N2, Clontech) containing a sequence encoding the α2-subunit integrin with a C-terminal RFP fusion protein (Texas A&M University Biomedical Engineering); empty vector was used as a control. Cells were allowed to recover during 24 hours in medium containing no antibiotics. Transfection efficiency was assessed after 24 hours using an inverted fluorescence microscope and α2 integrin immunocytochemistry with appropriate primary and secondary antibodies (Millipore) added to cells fixed with 4% paraformaldehyde and permeabilized with 0.2% Triton-X.

VEGF ELISA analysis. Confluent microvascular brain endothelial cells were serum starved for 12 hours prior to treatment with DV with or without 20-minute pretreatment with α5β1 function blocking antibody. After 24 hours, VEGF ELISAs (Insight Genomics) were performed on the endothelial cell conditioned medium following the instructions of the manufacturer. In some conditions, cells were pretreated with α5β1 function blocking antibody (1 μg/ml). VEGF ELISA was also performed on stroke (the visibly identifiable area of infarct) brain tissue lysate from PSD 1, 3, 7, 13, and 15, obtained on each PSD 8 hours after treatment with PBS or DV.

Quantitative PCR. Mouse brain endothelial cells were serum starved and then treated with 1% IMDM with or without DV for 2 hours. The protocol from the RNeasy Mini Kit was followed (QIAGEN, catalog 74104). Samples were quantified using a spectrophotometer, and qualitative analysis was performed by running samples on a 1% agarose gel. First-strand cDNA synthesis used cloned AMV RT for RT-PCR. cDNA from each sample was prepared following the Invitrogen Cloned AMV Reverse Transcriptase protocol (catalog 12328-019). qPCR products included TaqMan Fast Universal PCR Master Mix (2×; Applied Biosystems), No AmpErase UNG (Invitrogen, catalog 4352042), MicroAmp Fast 96-Well Reaction Plate (0.1 ml; Applied Biosystems, catalog 4346907). Vascular endothelial growth factor A (assay ID Mm00437304_m1), GAPDH (Mm99999915_g1), and integrinα-5 (Mm00439797_m1) primers were used. The following were mixed to a final volume of 25 μl and added to TaqMan Fast 96-well Reaction Plate: Fast Universal PCR Master Mix, gene expression assay mix, cDNA, and H_2O. The amount of cDNA added for each gene expression was optimized so that the dCt was around 18 cycles. Once the reaction plate was complete, it was analyzed using an Applied Biosystems 7500 Fast Reverse transcriptase PCR system.

In vivo permeability assays. EB-labeled albumin permeability assays were performed following previously published protocols (56). Briefly, anesthetized mice were subjected to stroke as described above. After 2 hours of injury, the mice were reperfused and immediately treated (2 hours post-stroke time point) or allowed to recover for 6 hours or 22 hours (8-hour and 24-hour time points, respectively) prior to treatment. Treatment consisted of i.p. injection of PBS or recombinant human DV (1 mg/kg, same dose as before) for 4 hours. Following treatment, 2% EB dye (preincubated with albumin) was administered by intravenous injection and was allowed to circulate for an additional 4 hours. The mice were sacrificed by cardiac perfusion with saline solution. Brains were rapidly removed. Sections (2-mm thickness) were used to calculate extravasated EB volume in infarct hemispheres. Additionally, the total amount of EB present in hemisphere homogenates (i.e., the extravasated amount of EB dye in μg/mg of brain tissue) was quantified by treatment with 300 μl formamide solution (Fluka Chemicals, Sigma-Aldrich) and incubation at 55°C for 3 days. Homogenates were centrifuged at 20,000 *g* for 10 minutes. Supernatants were used to quantify extracted EB by measuring absorbance at 620 nm. The total amount of EB was quantified using standard curves and normalized against hemisphere wet weight. Data are mean ± SD from 3 different animals.

In vitro OGD neuroprotection assays. For these experiments, the protocol of Li et al. (57) was adopted. The protocol is also presented schematically in Figure 6B. Mouse brain endothelial cells grown under routine cell culture conditions had their media removed (followed by 3 brief rinses with 1× PBS), followed by incubation in neuron media (DMEM-Hi glucose + PenStrep + B27) for 9 hours with or without DV (12.5 μg/ml) to generate brain endothelial cell conditioned medium. Additional neuron media with or without DV was added to empty wells not containing any cells as a media control. After 9 hours, the neuron and conditioned media were harvested and centrifuged for 10 minutes at 20,000 *g* to remove any cellular debris. The supernatant was collected, and a portion was analyzed for VEGF content via VEGF ELISA. The rest was frozen at –80°C until needed. Primary mouse cortical neurons were dissected from embryonic day 15 C57BL/6 mice. Neurons were plated in poly-D-lysine–coated 24-well plates. After 2 full days in culture, neurons were submitted to OGD (1% glucose, 90% N_2, 5% H_2, 5% CO_2, 37°C) for 2 hours in a hypoxia chamber (Billups-Rothenberg Inc.) and returned to a normal oxygen conditioned incubator (5% CO_2, 37°C) for reoxygenation. Following reoxygenation, the medium was removed and replaced with a 1:1 mix of the previously generated neuronal medium or the brain endothelial cell conditioned medium and fresh neuron medium with or without freshly added VEGF blocking antibody (1:100) or control IgG. After 24 hours, Alamar blue solution was

added and further incubated for 4 hours. Alamar blue fluorescence was measured as an indicator of neuronal viability with a fluorescent plate reader following instructions provided by the manufacturer. Briefly, fluorescence was measured with an excitation wavelength of 560 nm and emission wavelength of 590 nm.

DV α5β1 integrin binding assays. Binding assays were carried out using an optical biosensor (IAsys; Affinity Sensors) as described previously (58). In brief, to covalently bind the human α5β1 protein, designated as an acceptor, onto the surfaces of a sensor, we activated carboxylate groups present on the surface by injection of a 1:1 mixture of 0.1 M *N*-hydroxysuccinimide and 0.4 M *N*-ethyl-3-(3-dimethylaminopropyl) carbodiimide (Pierce). The acceptor dissolved in PBS was then allowed to bind to the activated surface until a response plateau was reached. The residual active groups were blocked by an injection of 100 μl of 1 M Tris-HCl (pH 8.5).

A cuvette with immobilized α5β1 was primed with the binding buffer (150 mM NaCl, 25 mM Tris-HCl, pH 7.4, and 1 mM $MnCl_2$). Free DV interactant dissolved in the binding buffer was added to the cuvette, and then the association phase was recorded. The sample was removed, analyte-free buffer was added to the cuvette, and the dissociation phase was recorded.

For binding assays, free DV was added at concentrations ranging from 8.0×10^{-8} M to 4.0×10^{-7} M. Data from the biosensor were analyzed by the global fitting method described by Myszka and Morton (59). For each assay, the association rate constants (K_{on}) and the dissociation rate constants (K_{off}) were obtained, and the equilibrium dissociation constant (K_d) values were calculated from a ratio of K_{off} to K_{on}. In addition, control binding of BSA at a molar concentration of 8.0×10^{-7} (double of the highest concentration for DV) was also performed.

Western immunoblots. Lysates were prepared from freshly frozen brains by incubation in RIPA lysis buffer complemented with protease inhibitor cocktail (Calbiochem, EMD Chemicals). Protein concentration was determined using the Bradford assay (Bio-Rad), and then samples containing 20 μg protein/well were loaded in 10% SDS-PAGE and transferred onto PVDF membranes. Membranes were incubating in blocking buffer (5% nonfat dry milk/TBS) for 1 hour at room temperature, followed by an overnight incubation at 4°C in the presence of antibodies directed against DV (R&D Systems), VEGF (R&D Systems), His (GeneTex), α5 integrin (Millipore), and GAPDH (Abcam). Membranes were washed with TBS–0.1% Tween 20 and incubated in the presence of HRP-conjugated secondary antibody (GeneTex). Band detection was performed by enhanced chemiluminescent substrate (SuperSignal West Pico, Thermo-Fisher Scientific) and captured by X-ray films. Blot quantification was performed using NIH ImageJ software.

Statistics. For all described experiments, unless otherwise stated, $n = 15$ (5 separate experiments, experiments for each condition performed in triplicate). Data are presented as mean ± SD (unless otherwise stated). Statistical significance ($P < 0.05$) was determined for all experiments by 1-way ANOVA, followed by the Dunnett post-test to compare experimental versus control conditions or the Bonferroni test to compare between different experimental conditions, using Prism 4.0 statistical package (GraphPad Software). Repeated-measures ANOVA using the Prism statistical package was used for comparisons between various treatment groups in motor function experiments. For anastomosis comparisons between littermate WT and $Pln^{-/-}$ mice, the interstain difference in the distance of the line of anastomoses from the midline was analyzed by 1-way ANOVA followed by Scheffe's post hoc test (22), and differences in the number of anastomoses were analyzed with Mann-Whitney *U* test (22).

Study approval. All animal experiments were approved by the IACUC of Texas A&M College of Medicine.

Acknowledgments

This work was supported by the American Heart Association, the Ted Nash Long Life Foundation, Texas A&M funding, and NIH grants R01NS065842-01A01 (to G. Bix) and 5R01AR049537-06 and 5R01AR048544 (to A. Fertala). We thank Jane Welsh and Jianrong Li for help with cell culture; Farida Sohrabji for training in the endothelin-1 stroke model; Tina Gumienny for the use of her confocal microscope; Sarah Bondos, Gregg Wells, Geoffrey Kapler, Siegfried Musser, Sumana Datta, Gregory Del Zoppo, Richard Milner, Eng Lo, Xiaoying Wang, Andrew Clarkson, and S. Thomas Carmichael for helpful discussions; Maurizio Mongiat for providing the pCep-pu vector for DV cloning; Jarek Aronowski for helpful discussions and training in the tandem ipsilateral CCA and MCA occlusion model; Martin Humphries for providing important reagents; and Paul Lockman for assistance with DV microscopy.

Received for publication January 10, 2011, and accepted in revised form May 18, 2011.

Address correspondence to: Gregory J. Bix, Molecular and Cellular Medicine Department, Texas A&M College of Medicine, 440 Reynolds Medical Building, College Station, Texas 77843, USA. Phone: 979.862.7613; Fax: 979.847.9481; E-mail: gjbix@medicine.tamhsc.edu.

1. Lo EM, Dalkara T, Moskowitz MA. Mechanisms, challenges and opportunities in stroke. *Nat Rev Neurosci.* 2003;4(5):399–415.
2. Lo EH. A new penumbra: transitioning from injury into repair after stroke. *Nat Med.* 2008;14(5):497–500.
3. Guo S, et al. Neuroprotection via matrix-trophic coupling between cerebral endothelial cells and neurons. *Proc Natl Acad Sci U S A.* 2008;105(21):7582–7587.
4. Ohab JJ, Fleming S, Blesch A, Carmichael ST. A neurovascular niche for neurogenesis after stroke. *J Neurosci.* 2006;26(50):13007–13016.
5. Chen J, Cui X, Zacharek A, Chopp M. Increasing Ang1/Tie2 expression by simvastatin treatment induces vascular stabilization and neuroblast migration after stroke. *J Cell Mol Med.* 2009;13(7):1348–1357.
6. Yao R, Zhang L, Wang W, Li L. Cornel iridoid glycoside promotes neurogenesis and angiogenesis and improves neurological function after focal cerebral ischemia in rats. *Brain Res Bull.* 2009;79(1):69–76.
7. Zhang ZG, et al. VEGF enhances angiogenesis and promotes blood-brain barrier leakage in the ischemic brain. *J Clin Invest.* 2000;106(7):829–838.
8. Hansen TM, Moss AT, Brindle NP. Vascular endothelial growth factor and angiopoietins in neurovascular regeneration and protection following stroke. *Curr Neurovasc Res.* 2008;5(4):236–245.
9. Sun Y, et al. VEGF-induced neuroprotection, neurogenesis, and angiogenesis after focal cerebral ischemia. *J Clin Invest.* 2003;111(12):1843–1851.
10. Bix G, Iozzo RV. Matrix revolutions: "tails" of basement-membrane components with angiostatic functions. *Trends Cell Biol.* 2005;15(1):52–60.
11. Fukuda S, et al. Focal cerebral ischemia induces active proteases that degrade microvascular matrix. *Stroke.* 2004;35(4):998–1004.
12. Giros A, Morante J, Gil-Sanz C, Fairen A, Costell M. Perlecan controls neurogenesis in the developing telencephalon. *BMC Dev Biol.* 2007;7:29.
13. Bix G, et al. Endorepellin causes endothelial cell disassembly of actin cytoskeleton and focal adhesions through α2β1 integrin. *J Cell Biol.* 2004; 166(1):97–109.
14. Bix G, et al. Endorepellin in vivo: targeting the tumor vasculature and retarding cancer growth and metabolism. *J Natl Cancer Inst.* 2006;98(22):1634–1646.
15. McGeer PL, Zhu SG, Dedhar S. Immunostaining of human brain capillaries by antibodies to very late antigens. *J Neuroimmunol.* 1990;26(3):213–218.
16. Sharkey J, Richie IM, Kelly PA. Perivascular microapplication of endothelin-1: a new model of focal cerebral ischaemia in the rat. *J Cereb Blood Flow Metab.* 1993;13(5):865–871.
17. Aronowski J, Grotta JC, Strong R, Waxham MN. Interplay between the gamma isoform of PKC and calcineurin in regulation of vulnerability to focal cerebral ischemia. *J Cereb Blood Flow Metab.* 2000; 20(2):343–349.
18. Bix G, Iozzo RV. Novel interactions of perlecan: unraveling perlecan's role in angiogenesis. *Microsc Res Tech.* 2008;71(5):339–348.
19. Rodgers KD, Sasaki T, Aszodi A, Jacenko O. Reduced perlecan in mice results in chondrodysplasia resembling Schwartz-Jampel syndrome. *Hum Mol Genet.* 2007;16(5):515–528.
20. Stum M, Davoine CS, Fontaine B, Nicole S. Schwartz-Jampel syndrome and perlecan deficiency. *Acta Myol.* 2005;24(2):89–92.
21. Arikawa-Hirasawa E, et al. Dyssegmental dysplasia, Silverman-Handmaker type, is caused by function-

al null mutations of the perlecan gene. *Nat Genet*. 2001;27(4):431–434.
22. Maeda K, Hata R, Hossmann KA. Differences in the cerebrovascular anatomy of C57Black/6 and SV129 mice. *Neuroreport*. 1998;9(7):1317–1319.
23. Maeda K, Hata R, Bader M, Walther T, Hossmann KA. Larger anastomoses in angiotensinogen-knockout mice attenuate metabolic disturbances after middle cerebral artery occlusion. *J Cereb Blood Flow Metab*. 1999;19(10):1092–1098.
24. Sakai T, et al. Plasma fibronectin supports neuronal survival and reduces brain injury following transient focal cerebral ischemia but is not essential for skin-wound healing and hemostasis. *Nat Med*. 2001; 7(3):324–330.
25. Schallert T, Fleming SM, Leasure JL, Tillerson JL, Bland ST. CNS plasticity and assessment of forelimb sensorimotor outcome in unilateral rat models of stroke, cortical ablation, parkinsonism and spinal cord injury. *Neuropharmacology*. 2000;39(5):777–787.
26. Woodlee MT, Asseo-Garcia AM, Zhao X, Liu SJ, Jones TA, Schallert T. Testing forelimb placing "across the midline" reveals distinct, lesion-dependent patterns of recovery in rats. *Exp Neurol*. 2005;191(2):310–317.
27. Nystrom A, et al. Role of tyrosine phosphatase SHP-1 in the mechanism of endorepellin angiostatic activity. *Blood*. 2009;114(23):4897–4906.
28. Kaji T, et al. The vascular endothelial growth factor VEGF165 induces perlecan synthesis via VEGF receptor-2 in cultured human brain microvascular endothelial cells. *Biochim Biophys Acta*. 2006; 1760(9):1465–1474.
29. Hayashi T, Noshita N, Sugawara T, Chan PH. Temporal profile of angiogenesis and expression of related genes in the brain after ischemia. *J Cereb Blood Flow Metab*. 2003;23(2):166–180.
30. Drevs J, et al. PTK787/ZK 222584, a specific vascular endothelial growth factor-receptor tyrosine kinase inhibitor, affects the anatomy of the tumor vascular bed and the functional vascular properties as detected by dynamic enhanced magnetic resonance imaging. *Cancer Res*. 2002;62(14):4015–4022.
31. Bix G, et al. Endorepellin, the C-terminal angiostatic module of perlecan, enhances collagen-platelet responses via the α2β1 integrin receptor. *Blood*. 2007; 109(9):3745–3748.
32. Milner R, Hung S, Wang X, Berg GI, Spatz M, del Zoppo GJ. Responses of endothelial cell and astrocyte matrix-integrin receptors to ischemia mimic those observed in the neurovascular unit. *Stroke*. 2008; 39(1):191–197.
33. Brown JC, Sasaki T, Göhring W, Yamada E, Timpl R. The C-terminal domain V of perlecan promotes β1 integrin-mediated cell adhesion, binds heparin, nidogen and fibulin-2 and can be modified by glycosaminoglycans. *Eur J Biochem*. 1997;250(1):39–46.
34. Mongiat M, Sweeney S, San Antonio JD, Fu J, Iozzo RV. Endorepellin, a novel inhibitor of angiogenesis derived from the C terminus of perlecan. *J Biol Chem*. 2003;278(6):4238–4249.
35. Francis SE, et al. Central roles of alpha5beta1 integrin and fibronectin in vascular development in mouse embryos and embryoid bodies. *Arterioscler Thromb Vasc Biol*. 2002;22(6):927–933.
36. Koivunen E, Wang B, Ruoslahti E. Isolation of a highly specific ligand for the alpha 5 beta 1 integrin from a phage display library. *J Cell Biol*. 1994; 124(3):373–380.
37. Weston RM, Jones NM, Jarrott B, Callaway JK. Inflammatory cell infiltration after endothelin-1-induced cerebral ischemia: histochemical and myeloperoxidase correlation with temporal changes in brain injury. *J Cereb Blood Flow Metab*. 2007;27(1):100–114.
38. Du C, Hu R, Csernansky CA, Hsu CY, Choi DW. Very delayed infarction after mild focal cerebral ischemia: a role for apoptosis? *J Cereb Blood Flow Metab*. 1996;16(2):195–201.
39. Shee WL, Ong WY, Lim TM. Distribution of perlecan in mouse hippocampus following intracerebroventricular kainate injections. *Brain Res*. 1998; 799(2):292–300.
40. Hou Q, Ling L, Wang F, Xing S, Pei Z, Zeng J. Endostatin expression in neurons during the early stage of cerebral ischemia is associated with neuronal apoptotic cell death in adult hypertensive rat model of stroke. *Brain Res*. 2010;1311:182–188.
41. Aviezer D, Hecht D, Safran M, Eisinger M, David G, Yayon A. Perlecan, basal lamina proteoglycan, promotes basic fibroblast growth factor-receptor binding, mitogenesis, and angiogenesis. *Cell*. 1994; 79(6):1005–1013.
42. Ay H, Koroshetz W, Finklestein S. Potential usefulness of basic fibroblast growth factor as a treatment for stroke. *Cerebrovasc Dis*. 1999;9(3):131–135.
43. Chen B, Cheng Q, Yang K, Lyden PD. Thrombin mediates severe neurovascular injury during ischemia. *Stroke*. 2010;41(10):2348–2352.
44. Chen B, et al. Severe blood-brain barrier disruption and surrounding tissue injury. *Stroke*. 2009; 40(12):e666–e674.
45. Yang S, Osman N, Burch ML, Little PJ. Factors affecting proteoglycan synthesis and structure that modify the interaction with lipoproteins. *Clin Lipidol*. 2009;4(4):479–492.
46. Zheng W, et al. Purinergic receptor stimulation reduces cytotoxic edema and brain infarcts in mouse induced by photothrombosis by energizing glial mitochondria. *PLoS One*. 2010;5(12):e14401.
47. Yang R, et al. Substantially attenuated hemodynamic responses to Escherichia coli-derived vascular endothelial growth factor given by intravenous infusion compared with bolus injection. *J Pharmacol Exp Ther*. 1998;284(1):103–110.
48. Daneman R, Agaliiu D, Zhou L, Kuhnert F, Kuo C, Barres B. Wnt/beta-catenin signaling is required for CNS but not non-CNS angiogenesis. *Proc Natl Acad Sci U S A*. 2009;106(2):641–646.
49. Pilorget A, Annabi B, Bouzeghrane F, Marvaldi J, Luis J, Beliveau R. Inhibition of angiogenic properties of brain endothelial cells by platelet-derived sphingosine-1-phosphate. *J Cereb Blood Flow Metab*. 2005; 25(9):1171–1182.
50. del Zoppo G, Milner R. Integrin-matrix interactions in the cerebral microvasculature. *Arterioscler Thromb Vasc Biol*. 2006;25(9):1966–1975.
51. Choi S, et al. Cooperation between integrin alpha5 and tetraspan TM4SF5 regulates VEGF-mediated angiogenic activity. *Blood*. 2009;113(8):1845–1855.
52. Bayless KJ, Kwak HI, Su SC. Investigating endothelial invasion and sprouting behavior in three-dimensional collagen matrices. *Nat Protoc*. 2009;4(12):1888–1898.
53. Waxham MN, Grotta JC, Silva AJ, Strong R, Aronowski J. Ischemia-induced neuronal damage: a role for calcium/calmodulin-dependent protein kinase II. *J Cereb Blood Flow Metab*. 1996;16(1):1–6.
54. Aronowski J, Cho KH, Strong R, Grotta JC. Neurofilament proteolysis after focal ischemia; when do cells die after experimental stroke? *J Cereb Blood Flow Metab*. 1999;19(6):652–660.
55. Lundy E, Solik B, Frank R. Morphometric evaluation of brain infarcts in rats and gerbils. *J Pharmacol Methods*. 1986;16(3):201–214.
56. Ogunshola OO, Djonov V, Staudt R, Vogel J, Gassmann M. Chronic excessive erythrocytosis induces endothelial activation and damage in mouse brain. *Am J Physiol Regul Integr Comp Physiol*. 2006; 290(3):R678–R684.
57. Li W, et al. The impact of paracrine signaling in brain microvascular endothelial cells on the survival of neurons. *Brain Res*. 2009;1287:28–38.
58. Brittingham R, et al. Single amino acid substitutions in procollagen VII affect early stages of assembly of anchoring fibrils. *J Biol Chem*. 2005;280(1):191–198.
59. Myszka DG, Morton TA. CLAMP: a biosensor kinetic data analysis program. *Trends Biochem Sci*. 1998; 23(4):149–190.